

A novel absorption-based enclosed heat pump dryer with combining liquid desiccant dehumidification and mechanical vapor recompression: Case study and performance evaluation

Wei Su ^{a,*}, Dongxu Ma ^a, Zhifei Lu ^a, Weixue Jiang ^b, Feng Wang ^b, Zhang Xiaosong ^{c,d}

^a School of Energy and Power Engineering, Northeast Electric Power University, Jilin, 132012, China

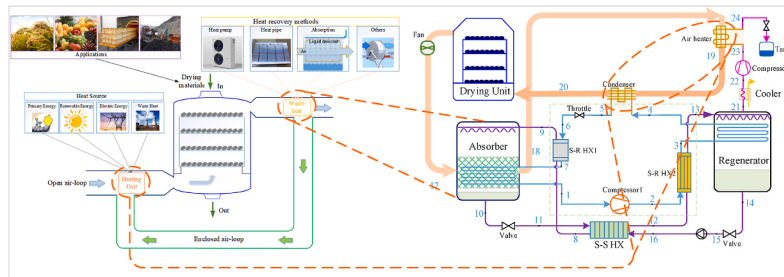
^b College of Electrical, Energy and Power Engineering, Yangzhou University, Yangzhou, 225127, China

^c School of Energy and Environment, Southeast University, Nanjing, 210096, China

^d Ministry of Education of Key Laboratory of Energy Thermal Conversion and Control, Southeast University, Nanjing, 210096, China



GRAPHICAL ABSTRACT



ARTICLE INFO

Keywords:

Liquid desiccant dehumidification
Heat pump
Waste heat recovery
Mechanical vapor compression
Drying

ABSTRACT

Drying process is ubiquitous and represents one of the most energy-intensive processes in varieties of agricultural, residential and industrial applications. As an effective heat recovery technology, the heat pump has recently been applied in various drying systems to provide heating and cooling, exhibiting good energy-saving potentials. However, existing condensing-based heat pump drying (HPD) systems require to significantly cool humid air for dehumidification, deteriorating energy efficiency. In this paper, an absorption-based enclosed HPD system is proposed to achieve total waste heat recovery by combining liquid desiccant dehumidification and mechanical vapor recompression. This study focuses on a comprehensive thermodynamic modeling and performance evaluation of proposed absorption-based HPD system. Analysis results indicate that the proposed system can deliver an energy utilization ratio of 4.54 and specific moisture extraction rate of 4.25 kg/kWh under design operation conditions, which is 18.7% and 18.5%

* Corresponding author.

E-mail address: weisu@neepu.edu.cn (W. Su).

higher than the traditional HPD system, respectively. Additionally, an economic analysis is adopted to appraise the economic performance, and obtained results show that the annual investment and maintenance cost rates of proposed system increases by 5.05%, but the annual operation cost rate is reduced by 19.94% compared to the reference system. The payback period is around 18.5monthes with a project life cycle of 20 years, which indicates that the project is profitable.

Nomenclature

| | |
|----------------------|--|
| <i>A</i> | area (m^2) |
| <i>CRF</i> | capital recovery factor |
| <i>Cp</i> | Specific heat |
| <i>Č</i> | cost rate(\$/year) |
| <i>d</i> | air moisture content(kg/kg) |
| <i>h</i> | enthalpy(kJ/kg) |
| <i>h_c</i> | heat transfer coefficient ($\text{kW}\cdot\text{m}^{-2}\cdot\text{K}^{-1}$) |
| <i>h_D</i> | mass transfer coefficient |
| <i>K</i> | over heat transfer coefficient ($\text{kW}\cdot\text{m}^{-2}\cdot\text{K}^{-1}$) |
| <i>m</i> | mass flow rate(kg/s) |
| <i>P</i> | pressure (kPa) |
| <i>Q</i> | heating capacity (kW) |
| <i>s</i> | specific entropy($\text{kJ}\cdot\text{kg}^{-1}\cdot\text{K}^{-1}$) |
| <i>T</i> | temperature ($^{\circ}\text{C}$) |
| <i>W</i> | electric power (kW) |
| <i>X</i> | mass fraction of solution |

Greek symbols

| | |
|------------|--|
| τ | annual system operation time (hour) |
| ω | humidity ratio(g/kg) |
| α | heat conductivity coefficient($\text{kW}\cdot\text{m}^{-2}\cdot\text{K}^{-1}$) |
| γ_k | maintenance factor |
| ρ | density(kg/m^3) |
| η | compression volume efficiency |
| ϵ | effectiveness |

Subscripts

| | |
|--------------|------------------|
| <i>a</i> | air |
| <i>abs</i> | absorber |
| <i>con</i> | condensation |
| <i>com</i> | compressor |
| <i>de</i> | dehumidification |
| <i>ex</i> | exhaust |
| <i>HX</i> | heat exchanger |
| <i>i</i> | inlet |
| <i>int</i> | internal |
| <i>lat</i> | latent |
| <i>o</i> | outlet |
| <i>pump</i> | pump |
| <i>r</i> | refrigerant |
| <i>ref</i> | refrigerant |
| <i>reg</i> | regenerator |
| <i>s</i> | solution |
| <i>sen</i> | sensible |
| <i>sys</i> | system |
| <i>tot</i> | total |
| <i>v</i> | vapor |
| <i>0,1,2</i> | state point |

Abbreviations

AEHPDD absorption-based enclosed heat pump drying system

| | |
|---------------|--|
| NTU | mass transfer unit |
| MRR | moisture removal rate |
| MVR | mechanical vapor recompression |
| COP | coefficient of performance |
| ICC | initial capital cost |
| EUR | energy utilization ratio |
| HX | heat exchanger |
| HPD | heat pump drying |
| RH | relative humidity |
| ODP | ozone depression potential |
| GWP | global warming potential |
| S-R XHHX | solution to refrigerant heat exchanger |
| S-S xx11HXHHX | solution to solution heat exchanger |
| SMER | specific moisture extraction rate |
| PBP | payback period |

1. Introduction

With increasing challenges of global energy dilemma and environmental problems, the improvement of energy utilization efficiency is becoming one of the most efficient ways to reduce energy consumption [1]. Over the last few decades, a large quantity of energy had been consumed by the vigorous development of industry, and thus special attention into improving energy efficiency should be focused on the most energy-intensive processes in industrial production [2,3]. Drying operation as one of the most important processes representing an energy-intensive procedure has been widely applied in various fields, such as agriculture, industry, residential or commercial applications, accounting for up to 15% of world's total energy consumption [4].

The objective of drying process is to take out the moisture from the wet products with a minimum cost and achieve maximum output, and consistently optimize these economic performance [4]. In conventional drying systems, industrial boilers driven by a fossil fuel, such as oil, coal, gas or direct electric heating facilities are the commonly used heating methods to produce high-temperature heating, typically with a maximum theoretical COP of 1 [5]. Currently, conventional drying facilities still dominate due to their lower capital cost and easily implementation in many industrial applications, but they suffer from low energy efficiency because of heat losses associated with hot air emissions. Considering the situation of global energy shortage and environmental pollution, it is of great importance to develop new drying technologies with high energy efficiency to be applied to reduce energy consumption.

Fig. 1 shows the schematic of basic drying system and flow cycles, which involves the critical facilities and commonly used heat recovery methods. Numerous studies indicated the usage of renewable energy contributed to decreasing energy consumption in dry

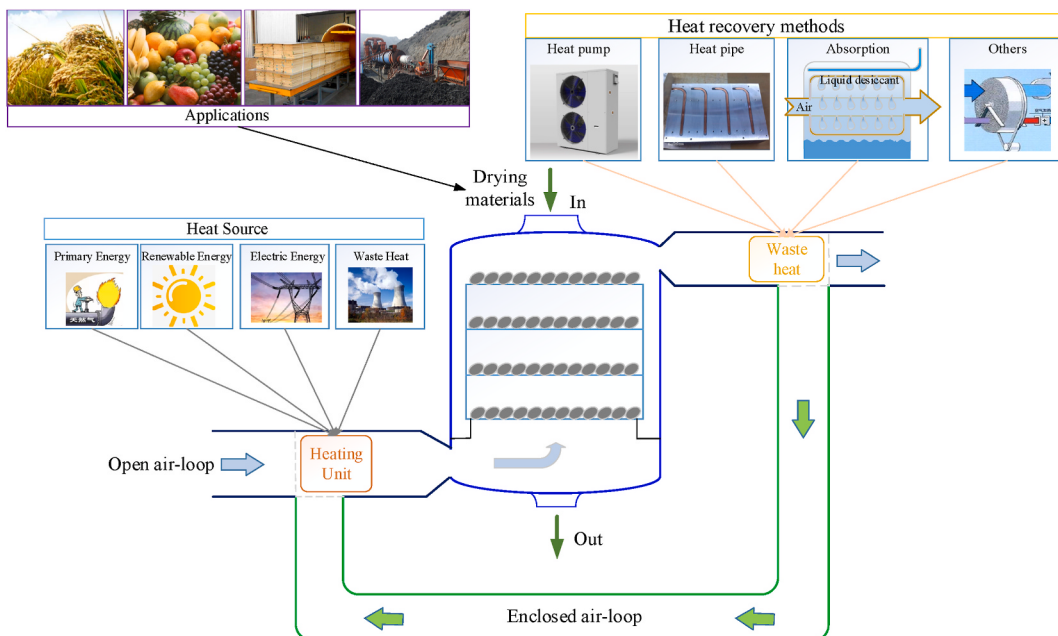


Fig. 1. Schematic of basic drying system and flow cycles.

operation and improving drying efficiency. Research, application and promotion of some new drying technologies, such as solar [6,7], heat pump [8,9] and their combination drying technologies [10,11] are increasing used for different places, like agricultural drying [12,13], gas clothes dryer [5], and industrial drying [14,15] all over the world. Moreover, exhaust air with a high humidity ratio produced during wet products drying process will be discharged into the environment in traditional dryers. Latent heat associated with humid gas, however, could be viewed as a potential renewable energy offering a unique way to improve energy efficiency and reduce energy use of various drying applications. Thus, the recovery of waste heat from exhausted moist gas is of great importance to improve the thermal efficiency of drying systems.

1.1. Review of heat pump drying systems

To reduce the energy consumption, heat pump drying systems, which could recover the low-grade waste heat and provide a high temperature heating output [16,17] have been considered as a promising drying technology due to its advantages of high efficiency, energy-saving and environmental protection. Especially, the heat pump drying (HPD) system is proven as effective drying method that ensure the dried product's quality for food or agricultural product owing to the adjustable drying temperature, humidity ratio (RH), drying rate and so on. Typically, the HPD system can be categorized into two groups: open air-loop cycle and enclosed air-loop cycle

Table 1
Summary of recent researches on various drying systems.

| Type | Year | Authors | Heat recovery methods | Open/closed | Methods | Application | Findings |
|--------------------------------|------|-------------------|-----------------------|-------------|-------------------------|------------------------------|--|
| Heat pump dryer | 2017 | TeGrotenhuis [22] | Heat pump | Closed | Simulation | Clothes drying | A hybrid HPD for clothes drying was developed by using off-the-shelf components capable of saving ~50% of the energy consumed by a traditional electrical heating dryer with comparable drying time based on a computation model. |
| | 2019 | Duan [17] | Heat pump | Closed | Experiment | Hawthorn cake drying | A new closed air cascade HPD system was proposed and experimentally studied, and the average SMER of the system was 0.94 kg/kW h which was much higher than hot air drying system. |
| | 2019 | Cranston [23] | Heat pump | Closed | Experiment & simulation | Washer dryer | A sorption bed was equipped between an evaporator and a condenser of the HPD to reduce energy consumption of the system. Theoretical investigation of the hybrid drying system showed that it could operate with 0.78 kWh and shorter drying time. |
| Solar dryer | 2016 | Daghighe [6] | Heat exchanger | Close | Experiment | – | A heat pipe evacuated tube solar dryer with heat recovery system was conducted to improve system efficiency and make full use of solar energy intake of the system. |
| | 2018 | Dorouzi [24] | Liquid desiccant | Closed | Experiment | Tomato slices drying | A PV-T solar collector was integrated with liquid desiccant-based system for tomato slices drying, which could provide the necessary electricity to meet the tomato drying require at temperature of 60–65 °C. |
| Heat pump assisted solar dryer | 2019 | Kuan [10] | Heat pump | Open | Simulation | Banana drying | Numerical models were proposed to examine the energy performance of a heat pump assisted solar dryer, and results indicated that, the hybrid drying system was more energy efficient than the traditional solar dryers. |
| | 2019 | Atalay [25] | Heat pump | Close | Simulation & experiment | Fruits and vegetables drying | The contribution of components in the solar dryer and heat pump dryer to system costs were analyzed in detail in terms of the exergoeconomic analysis, and it was found that the most important components needing to be improved are the fans in the solar dryer and the condensers in the heat pump dryer. |
| | 2020 | Singh [11] | Heat pump | Closed | Simulation & experiment | – | The convective enclosed solar-assisted HPD system was conducted and experimentally investigated for the drying of banana, and evaluated by comparing to simple HPD based on energetic and economic assessment. |
| | 2020 | Akhilesh [12] | Heat pump | Closed | Experiment | Banana chips drying | A new compact size convective batch-type solar-infrared assisted HPD system was presented and experimentally studied for enclosed air-loop drying of banana chips, results indicated the infrared-assisted HPD exhibited the lowest value of SMER. |

[4]. In open air-loop systems, the ambient air which is heated by condensers of heat pump systems flows into the drying chamber, and waste heat from the exhausted moist air can be recovered by evaporators of the heat pump. Much work so far has focus on the open air-loop HPD processes and relevant improved HPD systems. Aktas et al. [18] comparatively investigated the thermal characteristics and drying kinetic of a HPD system with and without infrared heaters. It was found that the infrared assisted heat pump dryer played prominent positive impact on the heat transfer efficiency, moisture content and drying rate, but energy consumption was raised by approximately a half. A solar assisted open air-loop HPD with less energy input and more controlled conditions was proposed by Seyfi et al. [19], in which products drying could be efficiently achieved with solar energy in daytime and the HPD system could be used for the rest of the time. According to reported studies on the open-loop drying method above, the fresh air was commonly heated to a high temperature by the heat pump. However, the applications of open air-loop HPD systems are limited in cold winter due to the extreme cold weather in some regions.

To overcome the shortcomings of open air-loop HPD systems mentioned above, enclosed air-loop HPD systems were proposed, in which the exhaust air from drying chamber was firstly cooled and dehumidified at the evaporator, and circulated back to condenser for heating and then returned the chamber to finish drying process. Enclosed air-loop HPD systems have the superiorities of effective humidity control and good hygienic conditions. By virtue of the dehumidification process, the drying medium could be recycled in the enclosed air channel, and would not be influenced by the environment, ensuring products' quality especially for food and agricultural products. Moreover, the pollution problem caused by exhaust gas emission can be avoided as well.

The application of enclosed air-loop HPD systems has wide prospects in many areas, and it is a good way to realize green drying process. Particularly, both of the heat pump's evaporation and condensation temperature are determined or affected by the drying process or demands. Therefore, special design of heat exchangers is indispensable to different drying application. Besides, the control strategy of heat pump systems is another crucial technology to assure the system efficiency and stability. Shi et al. [20] conducted a closed air HPD experiment to analyze the thin-layer drying kinetics of the yacon with drying temperature ranging from 5 to 45 °C and air flowrate of 0.5~2 m/s, and concluded that the drying temperature and air flowrate played a significant role on drying behavior of yacon slices. Chapchaimoh et al. [21] analyzed the drying performance and energy consumption of a closed air HPDS for a 50 °C drying temperature with air and nitrogen as the drying medium. Aktas et al. [9] presented a closed air HPD system for grape pomace drying applications at temperature of 40–50 °C. It was concluded that raising the temperature would decrease the drying time, system COP and specific energy consumption. Duan et al. [17] presented a new closed cascade HPD system, in which the hawthorn cake drying was taken as an example. Experimental results showed that the average COP of the cascade-like HPD system could reach ~3.45, and the energy consumption was decreased by 32.55% compared to a traditional hot air dryer.

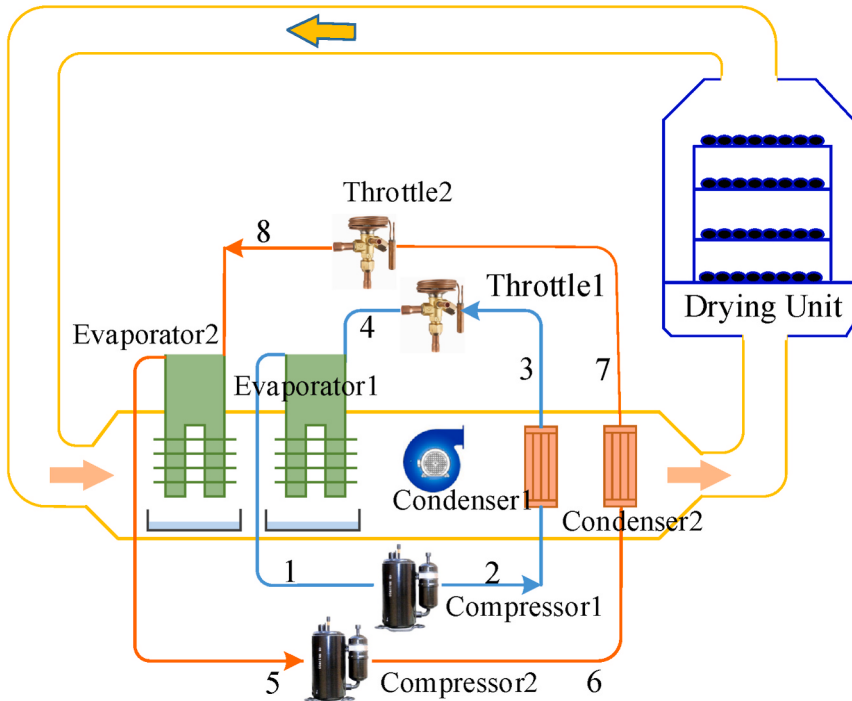
Existing heat pump based drying systems, however, need to significantly cool the air below its dew-point temperature for latent heat recovery. The necessary cooling and subsequent heating to the process air to a desired drying temperature will consume a large quantity of energy, thereby reducing energy utilization efficiency. Besides, researchers have conducted a number of studies on the combination of solar energy and heat pump heating to reduce energy consumption in dry applications and extend the using of renewable energy. The recent studies on heat pump and solar drying technologies are summarized as Table 1.

1.2. Review of heat recovery based on absorption

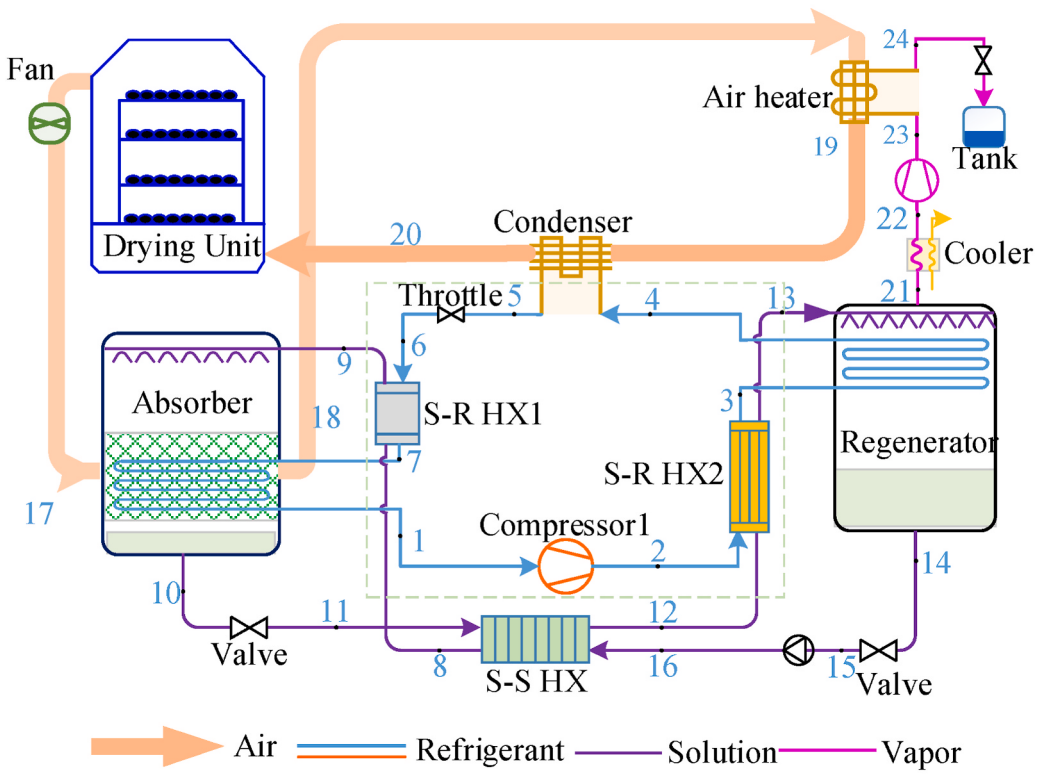
Up to now, condensation heat exchangers or condensing systems are the most commonly-used ways for waste heat recovery from the exhaust air in traditional HPD systems, which are directly equipped at the exit of the dryer [8,11,13]. However, the challenges of pressure drop, corrosion and fouling will strongly affect the performance of the heat exchangers [4,5]. Additionally, because exhaust gas needs to be significantly cooled below its dew point temperature for latent heat recovery, the heat recovery capacity of the condensation method immensely depends on the temperature of cooling medium. As a result, lower cooling temperature is required to recover more waste heat, especially the latent heat. The necessary cooling and reheating of the processed air will result in substantial energy consumption.

In the past decades, absorption-based system [16,26–28] attracts more and more attentions and has been considered as a promising way to recover the total heat of high humidity gas over traditional condensing cooling methods. The dehumidifier used in absorption-based system is a gas-to-solution direct contact heat and mass heat exchanger, in which the humid air comes into direct contact with some kind of liquid desiccant solution, generally LiBr–H₂O [29], CaCl₂–H₂O [30] or LiCl–H₂O. Due to the vapor pressure difference between the air and liquid desiccant, part of the moisture in the air is absorbed by liquid desiccant and the latent heat is able to be recovered at a relative high temperature, thereby overcoming the drawbacks of the traditional condensation method by which the water vapor condensing occurs only when the air temperature is lower than its dew-point temperature. Wang and Yang [31] proposed a hybrid heat recovery system by combining an open absorption heat pump with a multi-effect evaporation water desalination process, which was applicable to recover both latent heat and sensible heat of high humidity gases from the combustion of natural gas. The condensing heat exchanger and absorption heat pump were combined by Wang et al. [32] to recover the waste heat and water from the wet flue gas, by which around 70 MW of waste heat and 90 t/h of water could be simultaneously recovered with only a 5 °C temperature drop. A full-open absorption heat pump system was proposed by Yang et al. [33], and CaCl₂ and LiBr aqueous solution were selected as liquid desiccants for comparison. Results showed that the total heat recovery performance with two desiccants resulted to be similar, but CaCl₂–H₂O expended less initial investment cost because of its lower price.

The adsorption heat pump with zeolite-water as working pair was proposed and examined experimentally to generate steam for water [34,35]. Numerical simulation of the transport process for zeolite-water was conducted by Fukai et al. [35], and they concluded that raising water temperature rather than zeolite temperate is an efficient way to improve steam production. A novel sorption-based gas drying system was conducted by Ahmadi et al. [5] to improve waste energy recovery efficiency in exhaust gas from a clothes dryer, which achieved a 112% energy improvement compared with conventional gas clothes dryers. Cranston et al. [23] presented a



(a)



(b)

Fig. 2. Schematic of (a)two-stage cascade HPD system and (b) proposed absorption-based enclosed HPD system.

high-efficiency washer-dryer that embedded a heat pump for drying, and the energy efficiency was improved through hybridisation of the technology with a sorption bed. Results indicated that it was able to work with 0.78 kWh and shorter cycling time. However, it is difficult for the sorption bed to be continuous operation due to the periodic regeneration [36].

Given the multitude of various heat recovery applications published, it is observed that absorption-based system is a promising solution to improve the performance of HPD systems. However, the studies on liquid desiccant assistant heat pump drying systems are seldom presented in the open literatures.

1.3. Objective of present study

The above literature reviews clearly indicate that the development gaps for current HPD systems: (1) recovery of latent heat from exhaust air severely relies on the cooling temperature (dew point temperature), and the reheating of dehumidified air would also consume more extra heat energy, thereby limiting the system performance; (2) absorption-based heat recovery system is more effective in terms of round trip efficiency and economic benefit, while the combination of liquid desiccant dehumidification and enclosed air-loop heat pump system and their impact on the energy use still need further research; (3) regeneration of diluted desiccant solution, which is an energy-intensive process, should be carefully designed to achieve a better performance.

Given the above issues, this study aims to propose a novel absorption-based enclosed heat pump drying system (AEHPD), which enables to simultaneously dehumidify and heat the process air without cooling the air for dehumidification. Besides, a low-pressure regeneration system and a mechanical vapor recompression (MVR) device are employed to drive the liquid desiccant dehumidification cycle for effectively using latent heat associated with the water vapor as an advantageous heat source. Section 1 shows the research background, literature review, and objective of present study; Section 2 presents the configurations of reference and proposed system and working mechanism; Section 3 describes the mathematical models of proposed system; Section 4 provides the case study and parametric analysis; Section 5 presents the economic analysis; Section 6 concludes the main findings.

2. System description

2.1. Reference system

For enclosed air-loop HPD systems, both high condensation temperature and low evaporation temperature are required. However, the high pressure ratio of compressors may degrade system heating performance and even lead to an undesired shutdown of the heat pump [37]. The current permissible pressure ratio of compressors limits the drying temperature not high enough to satisfy the need of the drying. So, the enclosed cascade HPD system would be a promising alternative method to single stage enclosed HPD when a high drying temperature is required, such as higher than 75 °C [17]. Fig. 2(a) shows the system schematic of a representative two-stage cascade HPD system, which includes two separated heat pump units. Each heat pump unit is composed of an evaporator, a condenser, a throttle valve and a compressor.

The exhaust air from the drying chamber with high temperature and humidity will be successively cooled by evaporator 2 and evaporator 1 of heat pump units. After cooling and dehumidification in the evaporators, the low temperature and dried gas will be heated by condenser 1 and condenser 2 of heat pump units one after another. The configuration of cascade evaporators and condensers can reduce the pressure ratio of each heat pump. It should be mentioned that the condensing pressure is higher in heat pump unit 2

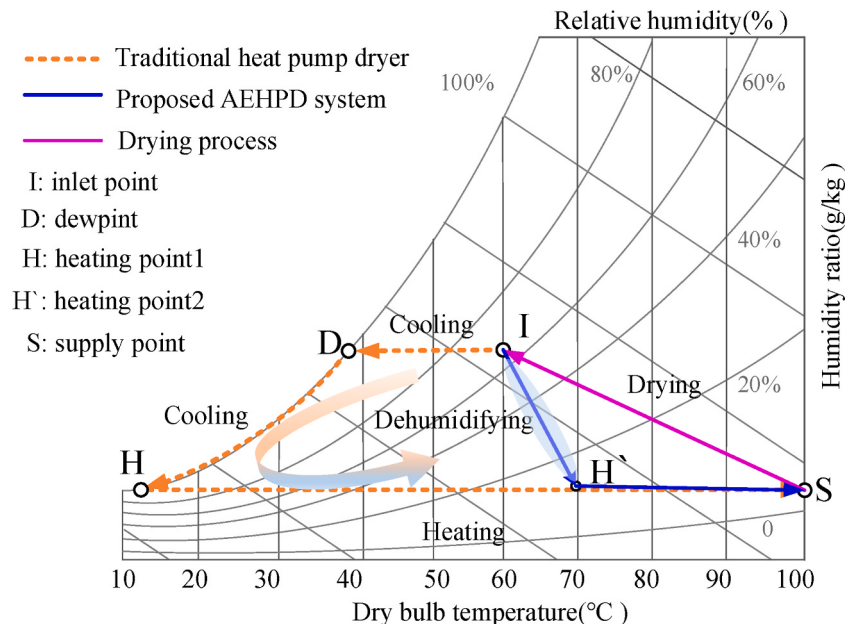


Fig. 3. Comparative psychrometric air flow processes of two drying systems.

while the corresponding evaporating pressure is higher as well. Similarly, the evaporating pressure is lower in heat pump unit 1 while the corresponding condensing pressure is lower as well.

In summary, the two-stage cascade enclosed air-loop HPD system is selected as reference systems for comparison with the absorption-based enclosed HPD system described in detail below.

2.2. Absorption-based enclosed HPD system

The proposed AEHPD system employs a novel method to effectively recover latent heat from the warm humid air at the exit of the drying unit, and reuse it to improve the system's energy efficiency. Fig. 2(b) exhibits the components and operation principles of the AEHPD system coupled with liquid desiccant dehumidification, vacuum-assisted regeneration and mechanical vapor recompression heating. As shown in Fig. 2(b), there are four sub-cycles in the AEHPD system, including the vapor-compression heat pump cycle, the solution dehumidification and regeneration cycle, the mechanical vapor recompression heating cycle and the gas circulation cycle.

For the heat pump cycle, it consists of compressor1, two solution to refrigerant heat exchangers (S-R HX1, S-R HX2), an absorber cooler, a throttling valve, a condenser, and a regenerator heater. The refrigerant is first compressed to high temperature vapor and successively pass through the S-R HX2, the regenerator heater and the condenser. After rejecting the heat to the solution and air, the refrigerant becomes subcooled liquid, and then goes into the throttling valve. Next, the refrigerant enters the S-R HX1, absorber cooler and is sucked by the compressor to achieve the refrigerant circulation.

In the air circuit, the exhaust air from drying unit is firstly dehumidified in the absorber, in which both the latent and sensible heat could be recovered by liquid desiccant, and then heated in the condenser and air heater. Along with the water absorption from humid air, the desiccant solution will gradually become weak, and cannot meet dehumidification requirement. Then the diluted solution is transferred to the regenerator, and achieves heat exchange with the strong solution from the regenerator in the solution-to-solution heat exchanger (S-S HX). Next, the diluted solution and strong solution will be further heated and cooled to the desired temperature in the S-R HX2 and S-R HX2, respectively. In the low-pressure regenerator the evaporating water steam is sucked into the compressor2 and compressed to the high pressure and temperature vapor, then releases the condensing heat to the process air.

Fig. 3 illustrates the air flow psychrometric processes of the two-stage HPD system and proposed AEHPD system. It is observed that in the traditional heat pump dryer, the air needs to be significantly cooled from point I to point H to achieve the dehumidification process, and subsequently heated to a desired drying temperature (process H to S). As shown, in the AEHPD system, the warm humid gas will be dehumidified via absorption process by liquid desiccant without any temperature reduction during dehumidification process, and meanwhile the latent heat recovered from the air can be used for the air and solution heating (process I to H'). Therefore, the proposed AEHPD system efficiently captures the waste heat of exhaust humid air and avoids extra cooling of the air, greatly improving drying energy efficiency.

3. Mathematical modeling

This study mainly focuses on a comprehensive thermodynamic and exergy modeling of the AEHPD system. In this section, the energetic, exergetic and economic models corresponding to the AEHPD system and traditional two-stage HPD system are developed, including the absorber model, regenerator model, the MVR model and heat pump cycle model. Solving the four interactive sub-models results in the calculation of important features of the AEHPD system, including the specific moisture extraction rate (SMER), energy utilization ratio (EUR), exergy efficiency (η_{ex}), coefficient of performance (COP) and so on, which will be presented in more detail in the following section.

To simplify the theoretical models, some assumptions are adopted as follows:

- (1) The heat losses and pressure drop of the refrigerant are assumed to be negligible in the pipeline and heat exchangers [29].
- (2) The desiccant solution is well-distributed in the packing materials, and wets the packed column and internal cooling coil completely [38].
- (3) There is no direct heat transfer between the humid air and the cooling coils.
- (4) The parameters of liquid desiccant and processed air in the control volume are identical [39].
- (5) The water vapor getting out of the regenerator is all saturated [40].

3.1. Energetic analysis model

3.1.1. Absorber model

In the absorber, liquid desiccant is sprayed from the top of the absorber, and directly contacts with humid air to achieve heat and mass transformation. In addition, the desiccant solution is cooled synchronously via heat exchange with the cooling coil. Thus, the mass transfer only occurs between liquid desiccant and air, the heat transfer occurs between desiccant and air, and between desiccant and the refrigerant.

In the present study, the typical *NTU-Le* model and finite element method (FEM) [39] are employed to establish the heat and moisture transfer models among the process gas, desiccant solution and low-temperature refrigerant in the absorber. The energy conservation equations can be written as follows [34,35,39]:

$$-\dot{m}_a dh_a + d(\dot{m}_s h_s) - \dot{m}_r dh_r = 0 \quad (1)$$

where \dot{m}_a , \dot{m}_s , \dot{m}_r is the mass flow rate of air, solution and refrigerant; h_a , h_s and h_r is the specific enthalpy of air, solution and refrigerant. The mass transfer between desiccant and the air is:

$$\dot{m}_a d\omega_a = d\dot{m}_s \quad (2)$$

where ω_a is the humidity ratio of air, The desiccant solution balance is given as:

$$d(\dot{m}_s X) = 0 \quad (3)$$

The heat transfer process between the desiccant and refrigerant is expressed in Eq. (4), where K_t and F_t represent the heat transfer coefficient and the area between the desiccant and refrigerant, respectively.

$$\frac{\partial Q_i}{\partial x dy} = \frac{K_t F_t}{H^* L} (t_s - t_{ref}) \quad (4)$$

The heat and mass governing equations between the air and desiccant solution can be expressed as follows [40].

$$d\omega_a = dNTU^*(\omega_s - \omega_a) \quad (5)$$

$$dT_a = dNTU^* Le^*(t_s - t_a) \quad (6)$$

$$dh_a = dNTU^* Le^* \left[(h_s - h_a) + \left(\frac{1}{Le} - 1 \right) * r * (\omega_s - \omega_a) \right] \quad (7)$$

$$dT_s = (Cp_s * T_s * m_a * d\omega_a - m_a * dh_a) / (m_s * Cp_s) \quad (8)$$

$$dX_s = m_a * d\omega_a * X_s / (m_s - m_a * d\omega_a) \quad (9)$$

where r is the vaporization latent heat of water, Cp_s is the specific heat of the solution, NTU is the number of mass transfer units and Le is the Lewis number, which is given as:

$$dNTU = \frac{h_D^* L^* dx^* dy}{m_a} \quad (10)$$

$$Le = \frac{h_c}{h_D^* Cp_a} \quad (11)$$

where h_c is the heat transfer coefficient; h_D is the mass transfer coefficient.

The boundary conditions are expressed as follows:

$$\begin{aligned} t_a &= t_{a,in}, \quad \omega_a = \omega_{a,in}, \quad h_a = h_{a,in}, \quad t_r = t_{r,in}, \quad \text{at } x = 0 \\ t_s &= t_{s,in}, \quad X = X_{in}, \quad \omega_c = \omega_{c,in}, \quad h_e = h_{e,in}, \quad \text{at } y = 0 \end{aligned} \quad (12)$$

Solving the above governing equations with boundary conditions gives the parameter distribution of air and solution in the absorber. The finite-difference numerical solution method is employed.

3.1.2. Regenerator model

The mathematical models of the regenerator are developed on the basis of energy and mass conservation, which are given as [40]:

$$m_{13} - m_{14} = m_{21} \quad (13)$$

$$m_r h_3 + m_{13} h_{13} = m_{14} h_{14} + m_r h_4 + m_{21} h_{21} \quad (14)$$

$$m_s c_{ps} \frac{dT_{reg}}{dt} = (KA)_{int,reg} (T_{con} - T_{reg}) - m_v (r + c_{p,v} (T_{con} - T_{reg})) \quad (15)$$

where r is latent heat of vaporization, m_v is mass flow rate of vapor, c_{ps} and $c_{p,v}$ are the specific heat capacity of solution and water vapor, respectively.

3.1.3. model

During the regeneration process, water vapor rejected from the desiccant solution still contains amount of latent heat, but its saturated temperature is relative low, limiting its use. In order to make full use of the waste heat, a mechanical vapor compressor is used to compress the vapor and subsequently condenses in a condenser for air heating. The heat and mass conservation equations listed below mathematically describe the MVR models.

$$m_{22} h_{22} + W_{com2} = m_{23} h_{23} \quad (16)$$

$$m_a h_{18} + m_{23} h_{23} = m_{19} h_{19} + m_{24} h_{24} \quad (17)$$

Vapor compressor is the core component of the MVR system, and the isentropic efficiency during the compression process is employed to predict the performance. The energy consumption of the compressor is given as follow [41]:

$$W_{\text{com2}} = m_v \frac{c_{p,v} T_i}{\eta_{\text{com2}}} \left(PR^{\left(\frac{\gamma-1}{\gamma}\right)} - 1 \right) \quad (18)$$

where η_{com2} is the isentropic efficiency, typically given as 0.75 [29]. PR is the pressure ratio of the compressor, γ is the polytropic exponent, W_{com2} is power consumption of compressor2.

3.1.4. Heat pump models

The heat pump in the proposed system is composed of four solution-refrigerant heat exchangers, a condenser, a throttle valve and a compressor. The models of each component can be integrated together based on the relationship among the component parameters to analysis the performance of the heat pump.

For the refrigerant compressor, the mass flow rate of the vapor or refrigerant into the compressor is given as [14]:

$$m_r = \frac{V_h \cdot \eta_v}{\nu} = \frac{n V_s \eta_v}{60 \nu} \quad (19)$$

where V_s is the working volume of the compressor, n is the rotate speed of compressor, ν is the vapor specific volume at the inlet of the compressor, η_v is the volume efficiency, which is calculated as [42]:

$$\eta_v = 0.959 - 0.006422 \frac{P_o}{P_i} \quad (20)$$

where P_0 and P_i are the outlet and inlet pressure of the compressor, respectively.

The energy consumption of the compressor1 can be expressed as follows [42]:

$$W_{\text{com1}} = \frac{m_r (h_o - h_i)}{\eta_{\text{com1}}} \quad (21)$$

The models of solution-refrigerant heat exchangers, condenser, air heater and some auxiliary components are listed in Table 2.

3.2. Exergy analysis model

The exergy analysis plays an important role in designing an efficient system and improving the performance of the existing system. Thus, in the present study, the exergy analysis is introduced to evaluate the performance of the proposed system. There are three fluids, involved refrigerant, desiccant solution and humid air in the proposed system.

The exergy value of the humid air at standard atmospheric pressure is the sum of the thermal exergy and humid exergy, and it can be expressed as [43]:

$$ex_a = c_{p,a} T_0 \left(\frac{T}{T_0} - 1 - \ln \frac{T}{T_0} \right) + R_a T_0 \left[(1 + 1.608\omega) \ln \frac{1 + 1.608\omega_0}{1 + 1.608\omega} + 1.608\omega \ln \frac{\omega}{\omega_0} \right] \quad (22)$$

where T and ω are the temperature and humidity ratio of the air, $c_{p,a}$ is the specific heat capacity of the air, and R_a is a gas constant for air. T_0 and ω_0 is the reference temperature and saturated humidity ratio [43].

Exergy of liquid desiccant solution is defined by Eq (23). in the form of a mole fraction, including physical and chemical exergy of liquid desiccant [43].

$$ex_s = ex_{ph}(T, P) + ex_{ch}(y_s, y_w) \quad (23)$$

Physical exergy can be expressed as:

Table 2
Key equations for heat pump system modeling.

| Components | Energy equations |
|----------------|--|
| Condenser | $m_r(h_4 - h_5) = m_a(h_{19} - h_{20}) = K_{\text{con}} A_{\text{con}} \Delta T, K_{\text{con}} = \left(\frac{1}{\alpha_r} + \frac{A_{\text{con},i}}{\alpha_a A_{\text{con},o}} \right)^{-1}$ |
| S-R HX1 | $m_r(h_7 - h_6) = m_s(h_8 - h_9) = K_{\text{HX1}} A_{\text{HX1}} \Delta T, K_{\text{HX1}} = \left(\frac{1}{\alpha_r} + \frac{A_{\text{HX1},i}}{\alpha_s A_{\text{HX1},o}} \right)^{-1}$ |
| S-R HX2 | $m_r(h_2 - h_3) = m_s(h_{13} - h_{12}) = K_{\text{HX2}} A_{\text{HX2}} \Delta T, K_{\text{HX2}} = \left(\frac{1}{\alpha_r} + \frac{A_{\text{HX2},i}}{\alpha_s A_{\text{HX2},o}} \right)^{-1}$ |
| Throttle valve | $h_5 = h_6$ |
| S-S HX | $m_{11}(h_{12} - h_{11}) = m_{16}(h_{16} - h_8), \varepsilon = (T_{12} - T_8)/(T_{16} - T_{11})$ |
| Air heater | $m_v(h_{23} - h_{24}) = m_a(h_{19} - h_{18}) = K_{\text{AHX}} A_{\text{AHX}} \Delta T, K_{\text{AHX}} = \left(\frac{1}{\alpha_v} + \frac{A_{\text{AHX},i}}{\alpha_a A_{\text{AHX},o}} \right)^{-1}$ |
| Pump | $W_{\text{Pump}} = \frac{m_s}{\eta_{\text{Pump}}} \left(\frac{\Delta P}{\rho_s} \right)$ |
| Fan | $W_{\text{Fan}} = \frac{m_a \Delta P_a}{\rho_a \eta_{\text{Fan}}}$ |

$$ex_{ph}(T, P) = h(T, P) - h^*(T_0, P_0) - T_0[s(T, P) - s^*(T_0, P_0)] \quad (24)$$

Chemical exergy can be expressed as:

$$ex_{ch,LiBr} = (1 / \bar{M}_{sol}) \left[\sum_{i=1}^n y_i \cdot \tilde{\epsilon}_i^0 + \bar{R} \cdot T_0 \sum_{i=1}^n y_i \cdot \ln a_i \right] \quad (25)$$

where \bar{M}_{sol} is the molar mass of the LiBr solution, $\tilde{\epsilon}_i^0$ is the standard chemical exergy for the LiBr and H₂O compounds, y_i is the mole fraction for LiBr or H₂O, a_i is the activity of the LiBr or H₂O.

Exergy destruction as a measurement of irreversibility in the heat and mass transfer process, could be determined by the inlet and outlet parameters of the components of the system as follow.

$$Ex_{des} = Ex_{in} - Ex_{out} \quad (26)$$

For a two-fluid heat exchanger, the exergy destruction inside can be calculated as [44]:

$$\Delta Ex_{hx} = \int T_0 \left(\frac{1}{T_h} - \frac{1}{T_c} \right) \cdot \delta Q_{hx} = \int \frac{T_0}{T_h T_c} \Delta T_{i,hx}^2 \cdot K_{hx} dF_{hx} \quad (27)$$

where T_0 denotes the reference temperature; T_h and T_c denote heating and cooling temperatures of two fluids in the heat exchanger, respectively; $\Delta T_{i,hx}$ denotes the difference of temperatures between the two fluids in a differential unit; and δQ_{hx} denotes the heat capacity transferred between the two fluids in a differential unit.

For the liquid dehumidifier, the exergy losses for heat transfer ($\Delta Ex_{abs,h}$) and mass transfer ($\Delta Ex_{abs,m}$) can be calculated by Eqs. (28) and (29), respectively:

$$\Delta Ex_{abs,h} = \int T_0 \left(\frac{1}{T_a} - \frac{1}{T_s} \right) \cdot \delta Q_{abs,h} = \int \frac{T_0}{T_a T_s} \Delta T_{i,abs}^2 \cdot K_{abs} dF_{abs} \quad (28)$$

$$\Delta Ex_{abs,m} = \int T_0 \left(\frac{1}{T_a} - \frac{1}{T_s} \right) \cdot \delta Q_{abs,m} = \int \frac{T_0}{T_a T_s} \Delta T_{i,abs}^2 \cdot \Delta \omega_{i,abs} K_{abs} dF_{abs} \quad (29)$$

where $\Delta T_{i,abs}$ denotes the difference between the temperatures of the two fluids in a differential unit; $\Delta \omega_{i,abs}$ denotes the difference between the air humidity ratio and desiccant's equivalent humidity ratio in a differential unit; and $\delta Q_{abs,h}$ and $\delta Q_{abs,m}$ denote sensible heat capacity and latent heat capacity transferred in a differential unit, respectively.

3.3. Economic model

As mentioned above, the proposed AEHPD system possibly achieves better energy efficiency, but results in more complicated system configuration and corresponding costs. Thus, a detailed economic analysis is required to estimate the payback period and the whole life cycle cost of such a system. In this section, a detailed economic analysis models consisting of the total annual capital cost rate and the payback period are developed.

3.3.1. Total annual capital cost rate

The total annual capital cost rate of the system is composed of the investment and maintenance cost rate of all components, and the operational cost rate, as shown in Eq. (30).

Table 3
Economic factor and investment and maintenance cost of each component [40,45,46].

| Equipment or factors | Correlations or economic index |
|---------------------------------|--|
| Compressor1 | $10167.5 \times W_1^{0.46}$ |
| Compressor2 | $7346 \times m_y \times PR \times \left(\frac{\eta_{com2}}{1 - \eta_{com2}} \right)^{0.7}$, where PR is pressure ratio |
| Evaporator or condenser | $2681 \times A_k^{0.59}$ |
| S-R HX, S-S HX | $2143 \times A_k^{0.514}$ |
| Absorber | $C_{cool,ab} + C_{packing,ab} = 2143 \times A_k^{0.514} + C_{ab} \times V_{ab}$ |
| Regenerator | $6570 \times \left(\frac{Q}{\Delta T} \right)^{0.8} \times 2 + 21276 \times m_{21} + 1184.4 \times m_{13}$ |
| throttle valve | $114.5 \times \dot{m}_r$ |
| pump | $705.48 \times \dot{W}_{pump}^{0.71} \times \left(1 + \frac{0.2}{1 - \eta_{pump}} \right)$ |
| Operation year of system(n) | 20 |
| Annual operation time(τ) | 4000 |
| Interest rate(i) | 10% |
| Maintain factor (γ_k) | 0.06 |

$$\dot{C}_{tot} = \dot{C}_{inv,main} + \dot{C}_{operation} \quad (30)$$

$\dot{C}_{inv,main}$ is the sum of the investment and maintenance cost rate of all components, which can be expressed by:

$$\dot{C}_{inv,main} = \sum_i \dot{C}_i \quad (31)$$

3.3.1.1. Investment and maintenance cost. The initial capital cost of each component in the system is of great significance for the economic analysis. The calculation equations of investment and maintenance cost for each component are listed in Table 3, which have been validated and commonly used in the previous literature.

For converting the initial capital cost to equal investment and maintenance cost rate during system whole lifetime, the annual investment and maintenance cost rate is expressed as [45]:

$$\dot{C}_i = C_i \times \gamma_k \times CRF \quad (32)$$

where γ_k is the maintenance factor, CRF is the capital recovery factor, shown as [45]:

$$CRF = \frac{i \times (1+i)^n}{(1+i)^n - 1} \quad (33)$$

where i is the interest rate, %, n is the lifetime of the component, as shown in Table 3 [47].

3.3.1.2. Operational cost. The annual operational cost rate of the AEHHD system can be expressed as follows:

$$\dot{C}_{operation} = \dot{W}_{sys} \times C_{ele} \times \tau \quad (34)$$

$$\dot{W}_{sys} = \dot{W}_{com1} + \dot{W}_{com2} + \dot{W}_{pump} + \dot{W}_{fan} \quad (35)$$

where \dot{W}_{sys} is the annual electric power consumption of the system, C_{ele} is the unit cost of electricity, τ is the annual operation time, h.

3.3.2. Payback period

The payback period (PBP) is the required time to return the investment and maintenance costs by income and salvage values, which can be determined by the ratio of the difference in the total cost to the difference in the operation cost. In the proposed AEHHD system, a new group of equipment including absorber, regenerator, S-R HX, S-S HX, MVR compressor and pump are required besides traditional heat pump system, for which we can calculate the payback period compared with the reference cascade HPD system. The income of the new system is the saved operational cost due to lower energy consumption, and the cost savings in investment and maintenance costs of heat pump due to the fact that with liquid desiccant and cycle improvement, the size of heat pump lessens.

The simple payback period can be summarized in the following equation [48].

$$PBP = \frac{ICC_{AEHHD} - ICC_{reference}}{(E + M)_{AEHHD} - (E + M)_{reference}} \quad (36)$$

where ICC is the initial capital cost, E is annual energy cost, M is annual maintenance cost.

3.4. Performance indexes

As mentioned above, the proposed AEHHD system investigated in this study aims to recover both latent and sensible heat and simultaneously provide a heating capacity for drying application. Metrics considered to characterize the performance of the proposed system are COP_{hp}, SMER, and EUR. All of the indexes are shown as follows:

$$COP_{hp} = \frac{Q_{con} + Q_{int,reg} + Q_{S-R,HX2}}{W_{com1}} \quad (37)$$

$$SMER = \frac{m_{water}}{\sum W} = \frac{m_{water}}{W_{com1} + W_{com2} + W_{fan} + W_{pump}} \quad (38)$$

$$EUR = \frac{m_{water} r + m_a c_{pa} (T_{20} - T_{17})}{\sum W} \quad (39)$$

The calculation of system exergy efficiency η_{ex} is shown as:

$$\eta_{ex} = \frac{Ex_{output}}{Ex_{input}} = \frac{Ex_{output}}{Ex_{output} + \Sigma \Delta Ex} \quad (40)$$

Additionally, in order to examine the dehumidification characteristic and heat recovery performance of the liquid desiccant in the absorber, we introduce moisture removal rate (MRR) and the dehumidification efficiency (η_{de}), which are calculated by:

$$MRR = \omega_{de,in} - \omega_{de,out} \quad (41)$$

$$\eta_{de} = \frac{\omega_{de,out}}{\omega_{equ}} \quad (42)$$

where ω_{equ} is equivalent humidity ratio of liquid desiccant. In the proposed AEHPD system, the heating and dehumidifying loads are defined as sensible and latent heat loads, which can be expressed as follows:

$$Q_{sen} = m_a C_{pa} (T_{20} - T_{17}) \quad (43)$$

$$Q_{lat} = (m_{17}\omega_{17} - m_{20}\omega_{20}) \times r \quad (44)$$

3.5. Simulation technique and working fluids selection

According to the mathematical models of each component, a modeling algorithm of the whole system is developed to combine four sub-cycles in Matlab software. Based on the predefined variables and four hypothetical initial parameters, the developed governing equations can be solved simultaneously via an iterative procedure with a small convergence of ~1%. The simulation starts with the absorber and regenerator, followed by the heat pump and mechanical vapor recompression. For the given inlet parameters of air and solution, outlet parameters can be got via the absorber model. The inlet solution temperature of the absorber is set as constant. The regenerator is used to concentrate the weak solution to its initial state to regain dehumidification ability. Therefore, the regeneration temperature (T_{13}) should be iterated so that the mass flow rate and concentration at Point 13 and Point 9 are within the allowed error range. Subsequently, the states of Point 12 and Point 8 can be determined by the S-S HX model. Finally, the required evaporation temperature, the dehumidification cooling capacity, the inlet and outlet solution temperature of the absorber can be obtained. Based on the condenser model, the heating capacity of condenser and S-R HX2 are obtained. Depending on the load matching, the air heater are activated accordingly. Following the energy balance, the refrigerant mass flow rate is updated. Finally, the performance metrics are available. The main outputs of the simulation include solution temperature, concentration, air temperature, air humidity, and overall performance indexes introduced before.

In proposed system, LiBr/H₂O solution is selected as liquid desiccant due to its stability, low cost and widespread application, and the properties of LiBr desiccant solution can be calculated by using the empirical formula developed in literature [49,50].

Different from traditional heat pump or refrigeration systems, the heat pump used in drying systems required to provide higher drying temperature, approximately 100 °C or more. Five environmentally friendly working fluids, including R514a, R245fa, R142b, R1234ze(z) and R600a are chosen as possible alternatives to HFCs to evaluate the performance of the proposed system. The thermodynamic properties of water vapor and refrigerants are obtained by the Chemours Company [51] and REFPROP9.1 [52], which are developed by NIST for getting the properties of various refrigerants. Table 4 presents the environmental indicators and properties of the five refrigerants. For environmental concerns, R514a, R245fa, R1234ze(z) and R600a exhibit zero ODP except for R142b with the ODP value of 0.043. Besides, R514a, R1234ze(z) and R600a have a very low GWP, while R142b and R245fa show much higher value.

A thermodynamic analysis of five alternative refrigerants in the proposed system were also conducted based on the developed simulation models at the same operation conditions. As shown in Table 4, R514a could be operated at the lowest pressure among the five refrigerant at the same evaporation and condensation temperatures, which means higher safety and lower requirement for the materials and manufacture. Moreover, the COP_{hp}, SMER and EUR of using R154a are higher than using R245fa, R142b, R1234ze(z) and R600a at the selected working conditions. Therefore, R154a is chosen as the working refrigerant in the proposed AEHPD system.

3.6. Validation

As far as the authors' knowledge, the proposed AEHPD system in present study has not been experimentally studied before. Accordingly, the developed mathematical models for the absorber, regenerator and heat pump driven liquid desiccant sub-cycle of the whole system are verified, separately. Liu et al. [53] experimentally analyzed an internally cooled liquid desiccant dehumidifier, in which the configuration and flow direction of solution to cooling water, air to solution and air to cooling medium are similar with the

Table 4
Properties and performance characteristics of alternative refrigerants.

| | R514A | R245fa | R142b | R1234ze(z) | R600a |
|-------------------------------------|--------|--------|---------|------------|--------|
| Boiling point (°C) | 29.1 | 15.3 | -9.3 | 9.7 | -11.7 |
| Molecular weight (g/mol) | 139.6 | 134 | 100.5 | 114 | 58.1 |
| Critical point (°C) | 178 | 154 | 137.2 | 150 | 135 |
| Critical pressure (MPa) | 3.52 | 3.6 | 4.12 | 3.5 | 3.65 |
| Heat of vaporization (kJ/kg) | 189 | 190 | 233 | 197 | 367 |
| Liquid density (kg/m ³) | 1322.2 | 1339 | 1107 | 1147 | 2064 |
| Specific heat (kJ/kg·K) | 1.14 | 0.92 | 1.34 | 0.758 | 1.31 |
| Thermal conductivity (W/m·K) | 0.129 | 0.0139 | 0.0094 | 0.086 | 0.019 |
| ODP | 0 | 0 | 0.043 | 0 | 0 |
| GWP | 2 | 1030 | 2400 | 6 | 20 |
| Low pressure (kPa) | 185.83 | 301.17 | 610.07 | 344.56 | 615.42 |
| High pressure (kPa) | 824.83 | 1327.5 | 2164.01 | 1413.6 | 1413.6 |
| COP _{hp} | 4.15 | 3.83 | 3.78 | 3.95 | 3.5 |
| SMER | 3.64 | 3.39 | 3.35 | 3.48 | 3.11 |
| EUR | 4.16 | 3.87 | 3.83 | 3.98 | 3.55 |

Table 5
Validation of dehumidification model.

| No | m_a (kg/s) | m_s (kg/ s) | X_{in} | $T_{cooling}$ (°C) | $Q_{cooling}$ (kW) | $T_{a,in}$ (°C) | $\omega_{a,in}$ (g/kg) | $T_{s,in}$ (°C) | $T_{a,out}$ (°C) | | | $T_{s,out}$ (°C) | | | $\omega_{a,out}$ (g/kg) | | | |
|----|-----------------|------------------|----------|-----------------------|-----------------------|--------------------|---------------------------|--------------------|------------------|-----------|-----------|------------------|-----------|-----------|-------------------------|-----------|-----------|-------|
| | | | | | | | | | Simulation | Ref. [53] | Deviation | Simulation | Ref. [53] | Deviation | Simulation | Ref. [53] | Deviation | |
| 14 | 1 | 0.178 | 0.059 | 0.410 | 13.90 | 1.89 | 33.8 | 15.2 | 29.9 | 28.1 | 2.49% | 27.9 | 28.6 | 2.51% | 13.1 | 13.9 | 6.11% | |
| | 2 | 0.178 | 0.058 | 0.401 | 17.60 | 1.68 | 34.0 | 15.7 | 31.5 | 29.5 | 2.37% | 29.2 | 30.1 | 3.08% | 14.5 | 15.3 | 5.52% | |
| | 3 | 0.139 | 0.056 | 0.397 | 13.45 | 3.26 | 35.0 | 17.7 | 29.5 | 28.9 | 1.38% | 28.7 | 29.6 | 3.14% | 14.1 | 14.7 | 4.26% | |
| | 4 | 0.177 | 0.055 | 0.407 | 13.95 | 3.05 | 35.9 | 18.5 | 30.7 | 30.2 | 29.8 | -1.32% | 30.3 | 29.6 | -2.31% | 15.0 | 15.9 | 6.00% |
| | 5 | 0.145 | 0.134 | 0.396 | 13.85 | 2.84 | 35.6 | 18.7 | 30.3 | 30.0 | 0.67% | 28.7 | 29.8 | 3.83% | 14.4 | 15.2 | 5.56% | |
| | 6 | 0.121 | 0.044 | 0.418 | 13.50 | 2.10 | 34.7 | 16.7 | 29.4 | 28.4 | 3.17% | 28.6 | 29.9 | 4.55% | 12.9 | 13.2 | 2.33% | |
| | 7 | 0.147 | 0.075 | 0.421 | 13.75 | 2.84 | 35.5 | 17.4 | 29.2 | 29.7 | 3.02% | 29.0 | 30.2 | 4.14% | 13.5 | 14.2 | 5.19% | |
| | 8 | 0.138 | 0.054 | 0.389 | 12.95 | 2.21 | 36.3 | 18.9 | 29.9 | 29.4 | 3.00% | 29.0 | 29.8 | 2.76% | 14.8 | 15.2 | 2.70% | |
| | 9 | 0.180 | 0.062 | 0.400 | 15.90 | 1.89 | 33.5 | 15.9 | 29.0 | 28.5 | 2.81% | 28.5 | 30.6 | 7.37% | 14.6 | 15.5 | 6.16% | |
| | 10 | 0.139 | 0.054 | 0.393 | 14.65 | 4.10 | 35.3 | 17.6 | 30.4 | 29.4 | 1.70% | 29.3 | 29.8 | 1.71% | 14.5 | 14.8 | 2.07% | |

absorber in present study. Thus, the experimental results from Ref. [53] can be used here to validate the present cross-flow internally cooling packed bed dehumidification module. Table 5 presents the comparison results between the present model and the available data from literature [53] for the internally cooling absorber. Three important output parameters, including $T_{a.out}$, $T_{s.out}$ and $\omega_{a.out}$ have been examined, and the maximum discrepancy of the predicted values were 3.17%, 7.37% and 6.16%, respectively, indicating the theoretical analysis can precisely express the performance of the absorber.

As to the heat pump driven liquid desiccant dehumidification system, the subject model is compared with a hybrid refrigeration system coupled with liquid desiccant dehumidification given by She et al. [54]. In their experimental study, the vapor-compression refrigeration supplied both cooling and heating for liquid desiccant dehumidification system, which is similar with present study. Therefore, experimental results from Ref. [54] could be used for modeling validation, and the simulation program is modified accordingly. Effects of mass flowrate of air (m_a), desiccant solution in the dehumidifier ($m_{s.de}$) and regenerator ($m_{s.reg}$) on The degree of subcooling (ΔT_{sub}), condensing temperature (T_{con}) and COP of the hybrid refrigeration system have been simulated, shown as Table 6. As can be seen, the relative errors of the simulation results are within $\pm 5\%$, indicating that the simulated models in this study are reliable and the simulated results could provide useful information.

4. Case study and parametric analyses

4.1. Case study

In this section, the performance of the proposed system under design operating conditions is examined by the developed models via a case study. The proposed AEHPD system aims to provide a low humidity and high temperature air for the enclosed grain drying system by recovering the waste heat from exhaust air. According to the design code for the grain drying in China, the initial moisture content of the grain is 20–25%, which should be reduced to 8–15%. The demanded drying rate is 1500 kg/h, and hence the total moisture removal rate in the dryer is 150–180 kg/h. Therefore, the system has supply/return air temperatures of 100/50 °C. Detailed operation conditions for the system are shown in Table 7. In the base-case, the mass fraction of LiBr solution is set to 60% and the generation pressure is set to 12 kPa for high efficient LiBr desiccant regeneration in low pressure conditions. Besides, the performance simulation of the reference system under the same operation condition was also conducted for comparison.

To clearly identify the thermodynamic process, the operation workflow of the drying flue gas and liquid desiccant in the proposed AEHPD system and two-stage cascade HPD system are depicted by a simplified diagram as shown in Fig. 4, in which the refrigerant cycle and heat pump system are omitted compared with Fig. 2. Fig. 4(a) indicates the thermodynamic states of the liquid desiccant (temperature and concentration) and air (temperature and humidity ratio) during system steady-state operation under design conditions. In the absorber, coupled heat and mass transfer occur between the processed air and liquid desiccant, and the humidity ratio of the air is reduced from 49.7 g/kg to 12.4 g/kg (RH decreased from 60% to 14%), while the air temperature reached 52.7 °C from 50 °C because it absorbs sensible heat released during the absorption process. Simultaneously, the concentration of liquid desiccant is decreased from 0.6 to 0.55, and the temperature of the solution increases from an initial temperature of 50.8 °C to a final temperature of 54.1 °C due to the absorption of latent heat. To achieve better dehumidification effectiveness, diluted solution needs to be regenerated via heating and boiling process in the regenerator. The solution temperature is increased to 87 °C and 100 °C by the S-S HX and S-R HX, respectively. For the reference system, as can be seen in Fig. 4 (b), the temperature of processed air is reduced from 50 °C to 35 °C and 17 °C by two cascade evaporators to achieve condensation dehumidification, and then the air is heated to 60 °C and 100 °C by the condensers, respectively.

The thermodynamic performances of the AEHPD system and reference system are summarized in Table 8. The total energy consumption of the AEHPD system is 64.14 kW, which provides 244.5 kW of heat capacity for solution and air heating. Run under the same

Table 6
Model validation results between present simulation and Ref. [54].

| m_a (kg/s) | ΔT_{sub} | | | T_{con} | | | COP | | |
|--------------------------------|------------------|------------|-----------|-----------|------------|-----------|-----------|------------|-----------|
| | Ref. [54] | Simulation | Deviation | Ref. [54] | Simulation | Deviation | Ref. [54] | Simulation | Deviation |
| 0.14 | 16 | 16.3 | 1.88% | 34.4 | 35.2 | 2.33% | 3.29 | 3.36 | 2.13% |
| 0.2 | 13.2 | 13.4 | 1.52% | 32.7 | 33.3 | 1.83% | 3.48 | 3.51 | 0.86% |
| 0.27 | 13.7 | 13.6 | -0.73% | 32.9 | 33.6 | 2.13% | 3.54 | 3.58 | 1.13% |
| 0.33 | 16.8 | 17.2 | 2.38% | 34 | 34.5 | 1.47% | 3.36 | 3.37 | 0.30% |
| <i>m_{s.de}(kg/s)</i> | | | | | | | | | |
| 0.33 | 17.9 | 18.6 | 3.91% | 38.3 | 37.7 | -1.57% | 3.4 | 3.5 | 2.91% |
| 0.41 | 18.1 | 18.5 | 2.21% | 38.5 | 38.4 | -0.26% | 3.47 | 3.6 | 2.31% |
| 0.49 | 18.3 | 19 | 3.83% | 38.5 | 38.9 | 1.04% | 3.5 | 3.6 | 3.14% |
| 0.57 | 18.5 | 19.3 | 4.32% | 38.6 | 39.4 | 2.07% | 3.54 | 3.7 | 3.96% |
| 0.65 | 18 | 18.7 | 3.89% | 38.1 | 38 | -0.26% | 3.59 | 3.8 | 4.74% |
| <i>m_{s.reg}(kg/s)</i> | | | | | | | | | |
| 0.4 | 18.2 | 18.5 | 1.65% | 39 | 39.6 | 1.54% | 2.9 | 2.96 | 2.07% |
| 0.52 | 18.1 | 18.3 | 1.10% | 38.6 | 39.1 | 1.30% | 3.1 | 3.15 | 1.61% |
| 0.66 | 18 | 18.4 | 2.22% | 38.2 | 38.6 | 1.05% | 3.13 | 3.18 | 1.60% |
| 0.73 | 18 | 18.5 | 2.78% | 38 | 38.3 | 0.79% | 3.27 | 3.32 | 1.53% |
| 0.85 | 18.1 | 18.6 | 2.76% | 38 | 37.9 | -0.26% | 3.28 | 3.38 | 3.05% |

Table 7
Baseline operation parameters and simulated conditions of studied system.

| Parameter | Baseline | Simulated conditions |
|--|----------|----------------------|
| Drying temperature (°C) | 100 | 80–100 |
| Exhausted air temperature (°C) | 50 | 40–60 |
| Exhausted air relative humidity (%) | 60 | 40–90 |
| Exhausted air humidity ratio (g/kg) | 49.7 | 31.9–76.6 |
| Air mass flowrate (kg/s) | 2 | 1–4 |
| Solution inlet temperature (°C) | 50 | 50 |
| Solution mass flowrate (kg/s) | 1 | 1 |
| Solution regeneration temperature (°C) | 100 | 100 |
| Solution concentration | 0.6 | 0.4–0.65 |
| S-S HX efficiency | 0.8 | 0.8 |
| NTU | 1.5 | 1.5 |

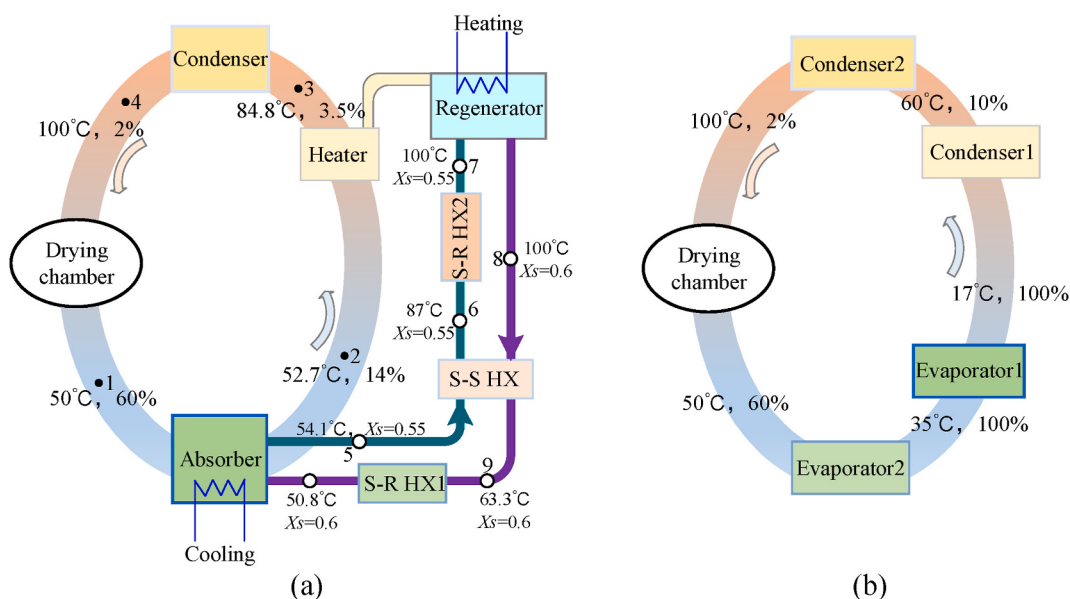


Fig. 4. Thermodynamic conditions of the air and liquid desiccant cycles of (a) proposed AEHPD system in present study (b) traditional two-stage cascade HPD system.

Table 8
Thermodynamic performances of the AEHPD system and reference system.

| Items | AEHPD system | Reference system |
|--|--------------|------------------|
| Refrigerant | R154a | R154a |
| Evaporation temperature (°C) | 48.8 | 32/13 |
| Condensation temperature (°C) | 103.6 | 103.6/52 |
| Moisture removal rate (g/s) | 74.6 | 74.6 |
| Absorption/condensation temperature (°C) | 52.7 | 17 |
| Cooling input (kW) | 197.9 | 225.7 |
| Heating input (kW) | 244.5 | 289.9 |
| Compressor power input (kW) | 62.95 | 75.5 |
| Pump power input (kW) | 0.54 | – |
| Fan power input (kW) | 0.65 | 0.45 |
| COP of heat pump | 4.45 | 3.84 |
| SMER | 4.25 | 3.58 |
| EUR | 4.54 | 3.83 |

condition, the energy consumption of the reference system is close to 75.95 kW, and cooling and heating inputs are 197.9 kW and 225.7 kW, respectively. This is because the air needs to be cooled to a lower temperature for condensation dehumidification, and subsequent reheating would consume more heat energy. Thus, the significant increase of 18.5% and 18.7% in the SMER and EUR of the proposed system can be observed over the reference HPD system.

4.2. Parametric analysis of the AEHPD system

In this section, to examine the performance of the AEHPD system for grain drying application in detail, parametric analysis is carried out under variable exhaust air temperature ($T_{a,ex}$) and relative humidity ($RH_{a,ex}$), solution mass flow rate (m_s) and concentration ($X_{s,ab}$), air mass flow rate (m_a) and drying air temperature ($T_{a,dry}$). The variation ranges of air parameters ($T_{a,ex}$, $RH_{a,ex}$ and $T_{a,dry}$) are determined by common grain drying conditions from literatures [55–57]. For latent recovery facility (absorber and regenerator), the selection of simulation conditions (m_s , $X_{s,ab}$) is based on operation conditions of conventional liquid desiccant dehumidification system from literatures [38,39,58]. Except for the investigated parameters, the other parameters are set the same as the base-case condition, as shown in Table 7. The dehumidification performance, COP_{hp} , η_{ex} , SMER and EUR of the system under each condition are evaluated.

4.2.1. Performance under different exhaust air temperatures

The effect of exhaust air temperature ($T_{a,ex}$) on the performance of the AEHPD system is analyzed with $T_{a,ex}$ increasing from 40 to 60 °C while the humidity ratio of exhaust air is kept constant at 45 g/kg. Fig. 5 (a) shows variations of the COP_{hp} , SMER, and EUR at different exhaust air temperatures. The values of COP_{hp} provide a measure of heating performance for the heat pump in proposed system. The SMER and EUR values represent the system energy efficiency considering the influences of heat load, moisture extraction rate and electrical energy input consumed by the compressors, pumps and fans. To better understanding the energy consumption of the system, Fig. 5(c) shows the effect of $T_{a,ex}$ on the energy consumption of the compressors and average heat loads of the drying process. As evident, at high exhaust air temperatures, the COP_{hp} and SMER performance metrics are high on account of the raised evaporation temperature and lower heat demand. As can be seen, different from COP_{hp} and SMER, the EUR decreases slightly from 4.33 to 4.16 as the exhaust air temperature increases from 40 to 60 °C. The reason for this change can be explained as follow: although both the energy consumption of compressors and total heat loads of the system reduce obviously (as shown in Fig. 5(c)), system heat loads exhibit a faster downtrend, leading to the reduction of EUR. Besides, both the energy consumption of two compressors and system heat loads decrease significantly with the increase of exhaust air temperature. Additionally, the latent heat of the system reduces slightly from 174.43 to 166.13 kW, while the sensible heat decreases obviously from 120.6 to 80.4 kW. This is because the exhaust air temperature makes a small impact on the dehumidification capacity of the proposed system, which is attributed to the latent heat loads of drying process. At high exhaust air temperature, the sensible heat loads are low due to the smaller temperature lift.

Fig. 5 (b) present the variations of exergy efficiency, exergy loss and exergy destruction of individual components in proposed systems with the increase of $T_{a,ex}$. When the inlet temperature of the absorber is increased, the moisture transfer from the exhaust air also increases, which in turn improves the cooling capacity and exergy gain of the exhaust air. However, this not only requires more heating energy at the regenerator but also needs more cooling energy at the evaporator. With input exergy exceeding the output exergy

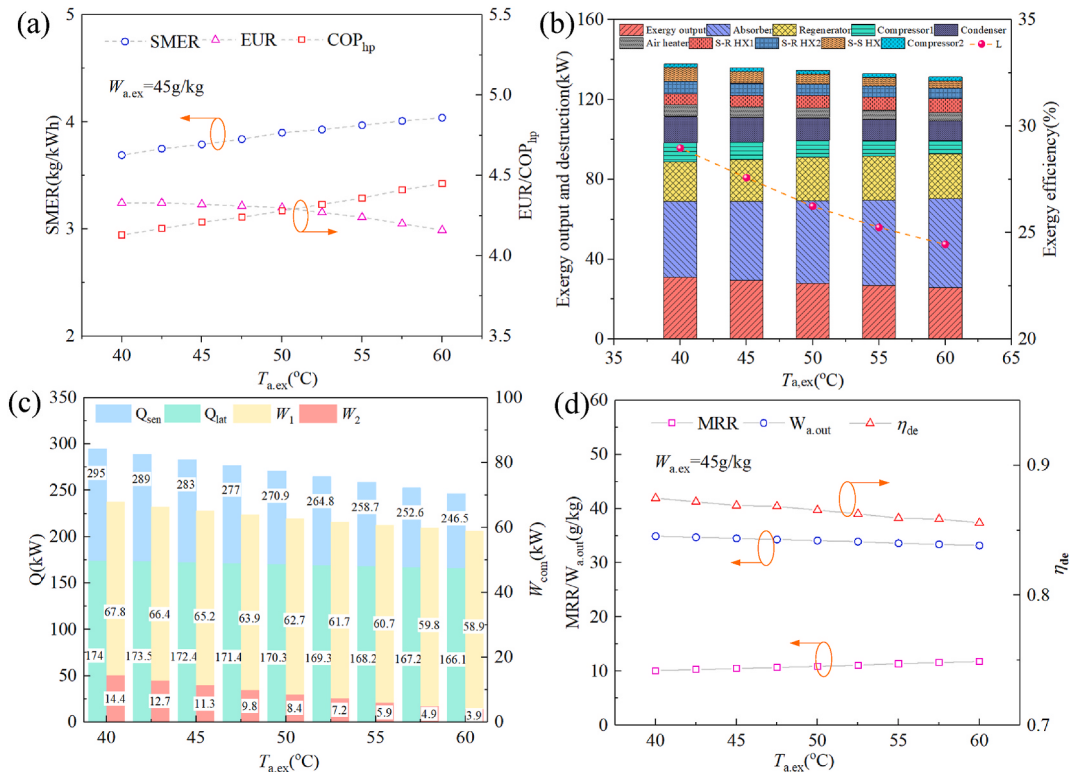


Fig. 5. Effect of the exhaust air temperature on the system performance.

gain, exergy efficiency of the proposed system decreases with the increase in the exhaust air temperature as shown in Fig. 5(b). The effect of the exhaust air temperature on the dehumidification performance of the absorber is also presented in Fig. 5(d). As shown, no significant changes are observed for both the MRR and outlet air humidity ($W_{a,out}$) when the air temperature increases from 40 to 60 °C. However, the dehumidification efficiency (η_{de}) of the absorber is reduced slightly from 87.5% to 85.5% as the air temperature rises. This is because the water vapor absorption rate of liquid desiccant and subsequent condensation rate are decreased with the increase of solution temperature.

4.2.2. Performance under different exhaust air relative humidity

Fig. 6 presents the effect of exhaust air relative humidity ($RH_{a,ex}$) on the performance of the AEHPD system. The variations of the COP_{hp}, SMER, and EUR are shown as Fig. 6 (a) with $RH_{a,ex}$ increasing from 40% to 90% while air temperature is kept constant at 50 °C. As the air RH increases, the moisture absorption rate increases and subsequent latent heat recovery boosts thereby improving the heat pump performance and energy utilization efficiency. Thus, all of the COP_{hp}, SMER and EUR performance metrics are improved when the $RH_{a,ex}$ increases. Particularly, the latent loads increase dramatically from 124.7 kW to 274.12 kW as the $RH_{a,ex}$ increases from 40% to 90%, and the ratio of latent loads to total heat loads is up to 73.18%. Similarly, the energy consumption of two compressors also increase from 57.55 kW to 68.55 kW because more heating energy is required for the diluted solution regeneration (as shown in Fig. 6 (c)).

Due to the increase of the moisture transfer in the absorber, both the cooling capacity and exergy gain of the exhaust air increase as the inlet air RH increases. Moreover, the increase in the desiccant temperature in the absorber decreases the heat transfer potential of S-S HX. The temperature of desiccant entering S-R HX2 therefore increases and consequently, the evaporation temperature of heat pump also increases. With the decrease in the input and increase in output, exergy efficiency of proposed system increases significantly for the studied air humidity as indicated in Fig. 6(b). Fig. 6(d) shows the effect of the exhaust air RH on the dehumidification performance of the absorber. As shown, the increase of the $RH_{a,ex}$ from 40% to 90% leads to the rise of MRR (from 25 g/kg to 54.8 g/kg) and outlet humidity ratio (from 7.3 g/kg to 22.9 g/kg). However, the dehumidification efficiency (η_{de}) of the absorber decreases gradually from 88.7% to 80.7% as the air RH increases. This is because more moisture will be absorbed from exhaust air as the $RH_{a,ex}$ increases, resulting in a quick drop of the liquid desiccant concentration. The thermodynamic analysis shows that the proposed AEHPD system can deliver a EUR of 5.44 and a SMER of 5.74 kg/kW·h at the high exhaust air humidity ratio of 90%, indicating that a better performance (COP_{hp}, SMER, and EUR) can be achieved at high air humidity ratio.

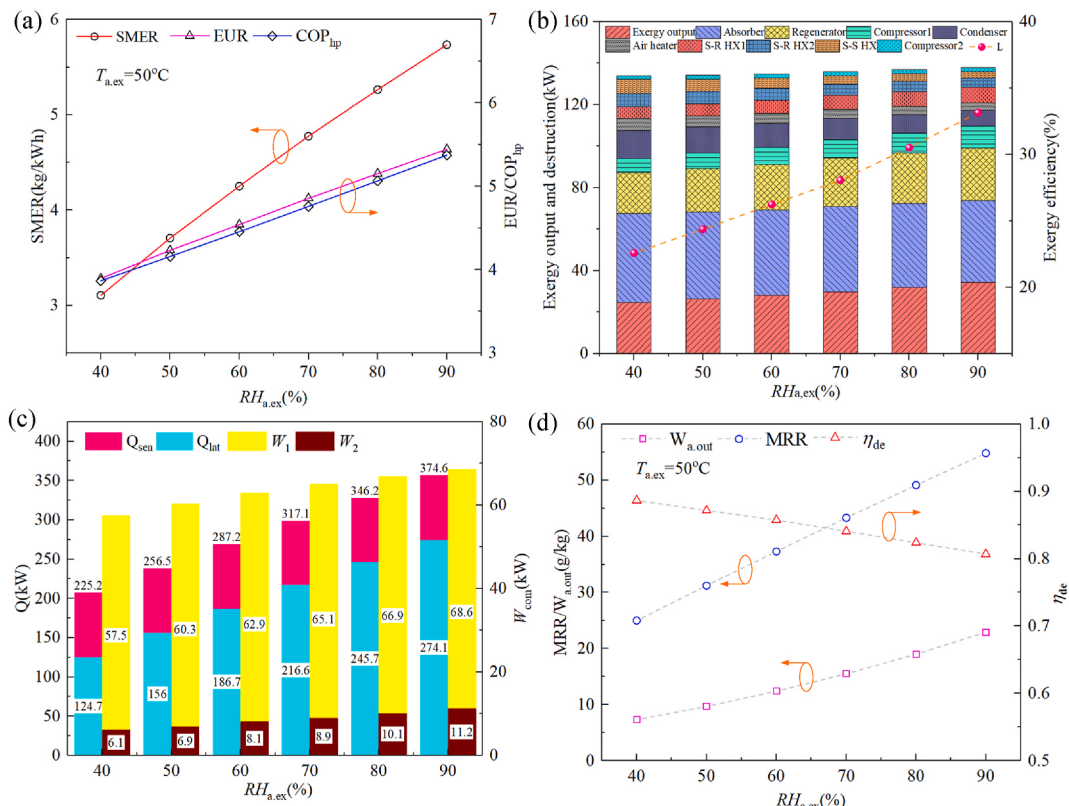


Fig. 6. Effects of the RH of air on the system performance.

4.2.3. Performance under different solution concentrations

The effect of the inlet solution concentration ($X_{s,ab}$) of the absorber on the system performance is conducted with the increase of $X_{s,ab}$ from 0.40 to 0.65 while the inlet air temperature is kept constant at 50 °C and the RH at 50%. Fig. 7 (a) shows variations of the COP_{hp}, SMER, and EUR at different inlet solution concentrations. The EUR and SMER increase when the solution concentration raises from 0.40 to 0.60. When solution concentration is close to 0.60, the SMER rates is moderate, but the EUR rate is maximized due to a high regeneration heat energy input. To better understanding the energy consumption of the system, the effect of $X_{s,ab}$ on the energy consumption of the compressors and average heat loads of the drying process is illustrated in Fig. 7(c). As evident, the energy consumption of two compressors increases significantly as the solution concentration increases. Additionally, the latent heat of the system increases significantly from 60.0 kW to 174.99 kW, while the sensible heat exhibits little changes. This is because the solution concentration plays an important role on the dehumidification capacity of the absorber, which is attributed to the latent heat loads of drying process.

Fig. 7(b) shows the exergy performances of the proposed system with the increase of solution concentration. As presented, exergy efficiency of proposed system firstly increases and then remains almost constant for the studied range. Because of the increase in the solution concentration and accordingly moisture transfer in the absorber, both the cooling capacity and exergy gain of the exhaust air increase. Moreover, the increase in the desiccant concentration improves the heat transfer potential of S-S HX. The cooling and heating capacities increase and consequently, the compressor energy consumption also increases. This leads to an increase in the energy and exergy input to the hybrid system. With the increase in both the input and output being more or less equal, exergy efficiency of the system remain almost constant when X_s is close to 0.6 as shown in Fig. 7(b). As can be seen in Fig. 7(d), the dehumidification efficiency (η_{de}) of the absorber is improved slightly from 86.4% to 89.3% with the increase of solution concentration. A high solution concentration can greatly improve the dehumidification capacity due to the MRR increase. Based on the above analysis, it is clear that the solution concentration plays significant effect on the system performance, and the EUR of the system is maximized at an intermediate solution concentration of 0.6.

4.2.4. Performance under different air-to-liquid flow rate ratios

Fig. 8 shows the effect of the air-to-liquid flow rate ratios (m_a/m_s) on the system performance with m_a/m_s increasing from 1.0 to 4.0 while the exhaust air is kept stable at temperature of 50 °C and RH of 50%. The variations of the COP_{hp}, SMER, and EUR at different exhaust air RH are shown in Fig. 8 (a). It can be found that both of the COP_{hp} and EUR performance metrics exhibit an upward trend as the m_a/m_s increases. As for the SMER, it becomes moderate when the m_a/m_s is close to 2.5, and will be maximized at an intermediate air-to-liquid flow rate of ~3.5. This is because the moisture absorption rate of liquid desiccant gradually decreases as the m_a/m_s increases, thereby reducing recovered latent heat and moisture extraction rate. Fig. 8(c) depicts the effect of the m_a/m_s on the energy

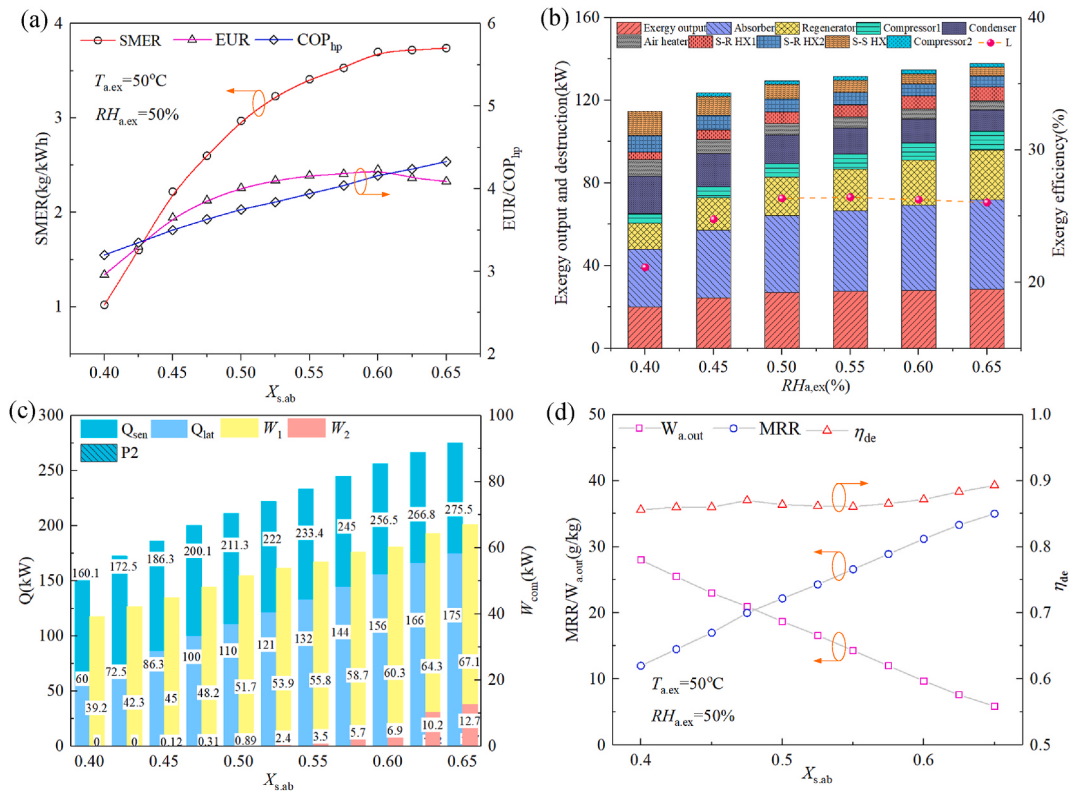


Fig. 7. Effect of the solution concentration on the system performance.

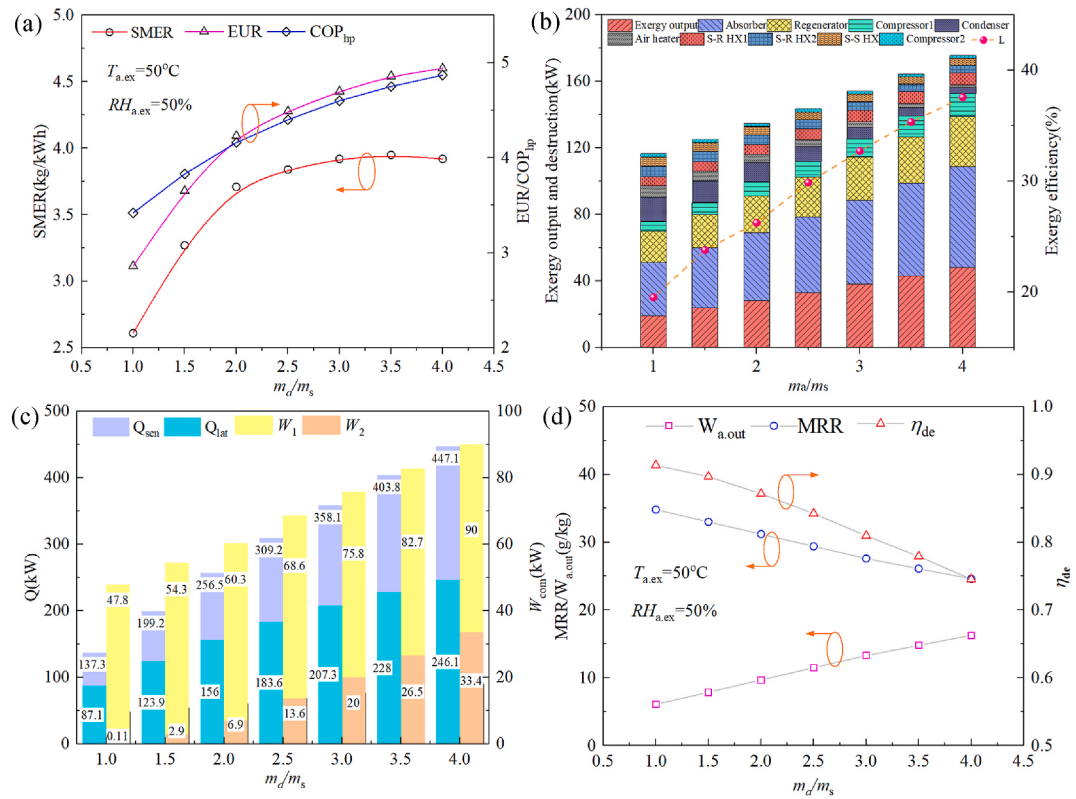


Fig. 8. Effect of the flow rate ratio of air-to-liquid on the system performance.

consumption of the compressors and average heat loads in the drying process. It is observed that both the latent heat load and sensible heat load increase obviously when the ratio of m_d/m_s increases, and the total heat load grows significantly from 137.31 kW to 447.14 kW. Additionally, the energy consumption of two compressors is also increased from 47.81 kW to 90.01 kW due to more heating energy required for the air heating and diluted solution regeneration.

When the air mass flow rate increases, it will transfer more moisture to desiccant solution in the absorber. It will also absorb more heat from the condenser in heat pump (Fig. 8(b)). Hence, both the exergy inputs and outputs increase. In addition, the exergy destruction of the process air decreases due to an increase in the exit temperature of the absorber. Therefore, the exergy efficiency of the proposed system increases with the increase of the air mass flow rate, as shown in Fig. 8(b). As shown in Fig. 8(d), when the m_d/m_s increases from 1.0 to 4.0, significant reductions of the MRR (from 34.8 g/kg to 24.6 g/kg) and dehumidification efficiency (from 91.3% to 74.5%) are observed. Furthermore, the final humidity ratio ($W_{a,out}$) is improved from 6.1 g/kg to 16.3 g/kg. This is because the higher air flow rate will reduce the contact areas and time between the air and liquid desiccant, leading to the reduction of the dehumidification efficiency and MRR. The analysis results indicates that the SMER of proposed AEHPD system peaks at an intermediate air-to-liquid flow rate of 3.5.

4.2.5. Performance under different drying temperatures

The effect of the drying temperature ($T_{a,dry}$) on the performance of the AEHPD system is analyzed with $T_{a,dry}$ increasing from 80 °C to 110 °C while the other parameters are kept constant, shown in Table 7. Generally, the condensation temperature of the heat pump and the regeneration temperature of liquid desiccant are determined by the values of $T_{a,dry}$. The variations of the COP_{hp}, SMER, and EUR at different drying temperatures are shown as Fig. 9 (a). It is obvious that all of the COP_{hp}, SMER and EUR performance metrics decrease rapidly as $T_{a,dry}$ increases. At high drying temperature, more heating energy is required in the proposed system. Additionally, both the heat pump and mechanical vapor recompression compressor need to provide a high condensation temperature for processed air heating, thereby degrading the system performance. Fig. 9(c) displays the effect of $T_{a,dry}$ on the energy consumption of the compressors and average heat loads of the drying process. As shown, with the increase of the $T_{a,dry}$ the sensible heat load increases significantly from 60.3 kW to 120.6 kW, while the latent heat is kept constant. In addition, the electrical energy consumed by the compressors rises 40.54 kW–73.24 kW, which is attributed to the increased sensible heat loads of drying process.

When the drying temperature is increased, it will absorb more heating from the condenser and air heater in heat pump system (Fig. 9(b)). Therefore, the exergy inputs increase in compressor1 and compressor2. Although the heating capacity and exergy gain of the supply air increase due to an increase of the air temperature, exergy output of the system increases slightly. Thus, exergy efficiency of the proposed system decreases with the increase of the drying temperature, as illustrated in Fig. 9(b). As can be seen in Fig. 9(d), there are no significant variations observed on the dehumidification efficiency (η_{de}), MRR and outlet humidity ratio ($W_{a,out}$) with the

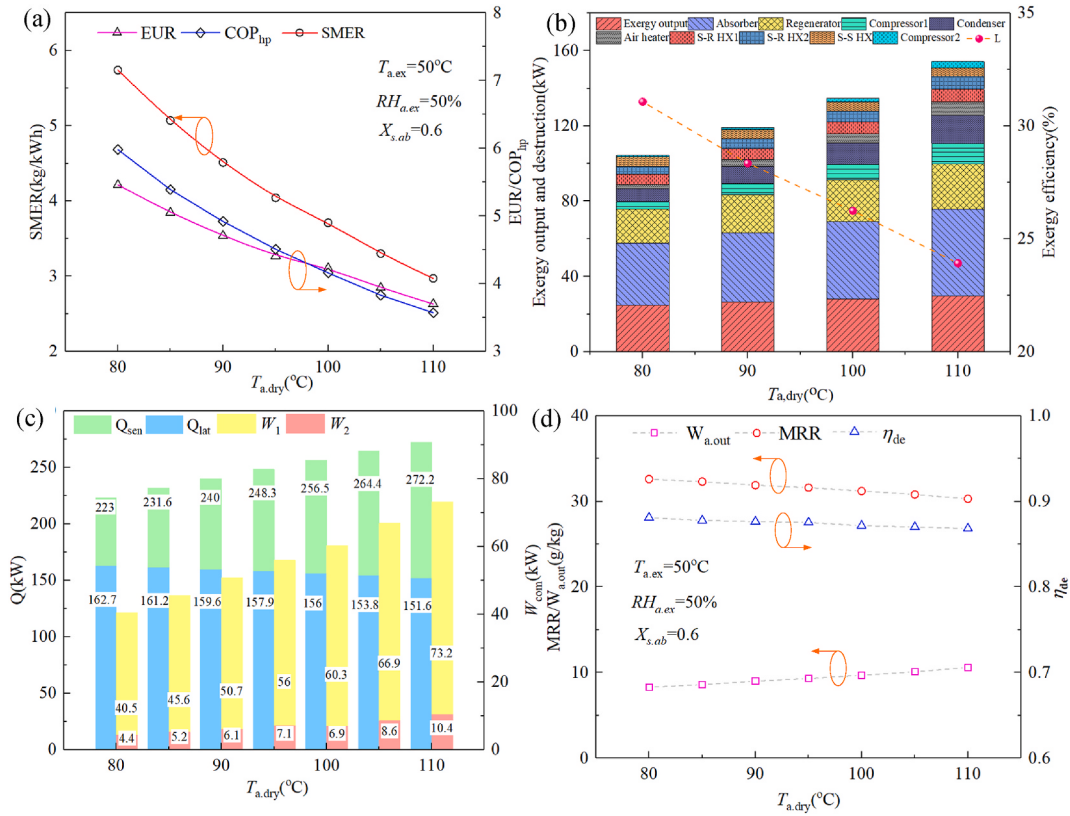


Fig. 9. Effect of the drying temperature on the system performance.

$T_{a,dry}$ increasing. This is because the dehumidification process in the absorber is not affected by the drying temperature of the proposed system. Based on the above analysis it can be seen that the drying temperature can negatively affect the system performance, but doesn't affect the dehumidification performance of the absorber.

4.3. Performance comparison with the enclosed air-loop HPD system

As mentioned in Fig. 3, the superiority of the proposed system has been analyzed from the perspective of thermodynamics in the psychrometric chart compared with the conventional enclosed HPD system. In order to further examine the performance improvement of the proposed system, a detailed comparative study is introduced in this section.

The inlet air humidity ratio of the drying unit plays a significant role on the materials drying time and drying efficiency, and a high mass transfer effectiveness can be obtained during most of the drying process under a lower air humidity ratio. Therefore, the dehumidification efficiency of the latent heat recovery system will directly affect both the SMER and EUR of the heat pump drying facilities.

Here, the performance comparison between the two-stage enclosed air-loop HPD system (shown as Fig. 2(a)) and the proposed system is conducted under different inlet air humidity ratios. For both systems, the average exhaust air temperature is 50 °C and the average air humidity ratio is 40.4 g/kg, and the drying air temperature sent into the drying unit is set as 100 °C with the humidity ratio increasing from 5.5 g/kg to 17.5 g/kg. The variations of the EUR and SMER under different inlet air humidity ratios for two systems are presented in Fig. 10(a). As can be seen, when the humidity ratio increases from 5.5 g/kg to 17.5 g/kg the SMER of the proposed system involves gradually drop (from 4.57 to 3.91), but the SMER of the reference system exhibits an upward trend from 3.11 to 3.56. It needs to be emphasized that the SMER of proposed system is 9.8%–46.9% higher than the two-stage cascade enclosed HPD system at chosen operation conditions. This is because for condensation dehumidification system a high evaporation temperature can offer a high air humidity ratio, thereby improving the COP of the heat pump. As for the absorption-based dehumidification system, the decreased moisture absorption will bring down the heat pump performance. Similarly, the EUR of the reference HPD system gradually goes up when the drying inlet air humidity ratio increases from 5.5 g/kg to 17.5 g/kg, while the EUR of the proposed system has a slight downward trend with the humidity ratio increasing, and the gap between reference system and AEPHD system gradually becomes narrowing. The comparison analysis indicates that the proposed system can achieve an energy-efficient latent heat recovery. However, its superiority will shrink with the increase of the dryer inlet air humidity ratio.

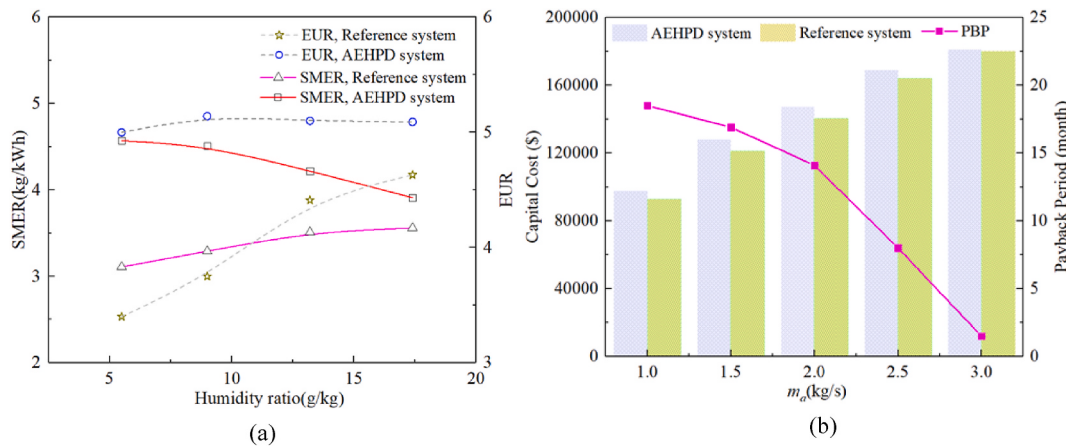


Fig. 10. (a) Performance comparison of proposed system and reference system; (b) the capital cost and payback period of the AEHPD system with different capacities.

5. Economic analysis

Based on the thermodynamic analyses, the proposed system exhibits a higher energy efficiency than the traditional enclosed HPD system but resulting in a more complicated system. Thus, it is necessary to examine its economic benefits. To determine the systems initial investment costs, the dry air mass flowrate is set as 2 kg/s, with the temperature of 100 °C, and humidity ratio of 10 g/kg. For both HPD systems mentioned above, the input is the electricity, while the outputs is dry and high-temperature air. The proposed system is considered with an operation life-span of 20 years and an operation of 4000 h/year, as shown in Table 3. The industry electricity rate is set as \$0.12/kWh.

The annual investment and maintenance cost rates of different components are shown in Table 9 for the two systems. The AEDHP system is more complicated than the traditional enclosed heat pump system, and the annual investment and maintenance cost rate of the AEDHP system is a little higher than that of the reference system. The majority of the proposed system cost is on the absorber, regenerator and compressor2. However, four heat exchangers take up the majority costs of the reference system. This is attributed to the lower heat transfer efficiency of the air heat exchangers, which increases the annual investment and maintenance cost rate of the reference system. Compared with the reference system, the total annual investment and maintenance cost rate of the AEDHP system increases by 5.05%, but the annual operation cost rate reduces by 19.94%.

The unit drying capacity of the system is determined by the air mass flow rate sent into the drying unit. Fig. 10(b) displays the capital cost and simple PBP of the proposed system with different air mass flow rates. A higher mass flow rate results in a higher capital cost in system components and thus a higher total capital cost, as Fig. 10(b) shows. However, the payback period of proposed system decreases significantly from 18.5 to 1.5 months with the increase of the air mass flow rate, indicating that a larger capacity is beneficial to the economic performance of the AEHPD system. It is mainly due to the fact that the economic benefits increase much faster than the investment and maintenance costs with the increasing of the system capacity. Besides, the proposed system has a much shorter payback period (1.5–18.5 months) compared with the reference system, indicating the AEHPD system is more superior in terms of

Table 9
Annual investment and maintenance cost rate of each component.

| Components | AEHPD system (\$/year) | Reference system (\$/year) |
|----------------|------------------------|----------------------------|
| Compressor1 | 486.2022 | 1204.865 |
| Compressor2 | 3113.506 | 3217.204 |
| Absorber | 3576.523 | – |
| Condenser1 | 1558.755 | 3882.557 |
| Condenser2 | – | 2932.414 |
| Evaporator1 | – | 3307.881 |
| Evaporator2 | – | 2711.223 |
| Air heater | 2262.531 | – |
| Air cooler | 622.538 | – |
| S-R HX1 | 652.7362 | – |
| S-R HX2 | 597.5524 | – |
| S-S HX | 709.2845 | – |
| Regenerator | 3948.295 | – |
| Throttle | 62.2538 | 99.60608 |
| Pump | 149.4091 | – |
| Pipe and valve | 622.538 | 124.5076 |
| Total | 18362.12 | 17480.26 |
| Operation cost | 30216 | 36240 |

economic benefits.

6. Conclusions

This study introduced a novel absorption-based enclosed heat pump drying system by combining liquid desiccant dehumidification and mechanical vapor recompression to overcome the drawbacks deteriorating energy efficiency in existing heat pump drying systems. Based on the developed mathematical models, detailed thermodynamic, exergic and economic analyses were carried out to evaluate the system performance. Particularly, a thorough parametric analysis was addressed to examine the influence of several significant parameters on the performance of proposed system. Besides, the working principles and performance comparison between the proposed system and reference system was also performed. Economic analysis showed the annual investment and maintenance cost rate of proposed system is a little higher than the reference system due to its complicated configuration, but the annual operation cost rate was reduced by 19.94%. With a project life-span of 20 years, the proposed system has a short payback period of 1.5–18.5 months, compared with the reference system. The proposed system may provide a feasible way to recover the latent heat from exhaust air as renewable energy sources, thereby promoting the energy efficiency of the heat pump drying system.

CRediT authorship contribution statement

Wei Su: Conceptualization, Methodology, Writing -original draft, Project administration. Dongxu Ma: Conceptualization, Methodology, Writing-review & editing. Zhifei Lu: Conceptualization, Software, Methodology. Weixue Jiang: Software, Investigation. Feng Wang: Writing-review & editing. Xiaosong Zhang: Supervision, Project administration.

Declaration of competing interest

The authors declare that they have no known competing financial interests or personal relationships that could have appeared to influence the work reported in this paper.

Acknowledgments

This work is supported by Projects of Science and Technology Development plan of Jilin Education (JJKH20210088KJ).

Appendix A. Supplementary data

Supplementary data to this article can be found online at <https://doi.org/10.1016/j.csite.2022.102091>.

Appendix

In this study, the fin-tube air heater and condenser are used in proposed system. The inner and outer diameters of the tubes in condenser and evaporator are 8.82 mm and 9.52 mm, respectively. The coil length may vary for changing the heat exchange area to meet different working conditions. The detailed specifications for air heater and condenser are shown in [Table A1](#).

Table A1
Main Specifications of the air heater and condenser

| Parameters | Values | Unit |
|-----------------------------|----------|------|
| Inner tube diameter | 8.82 | mm |
| Outer tube diameter | 9.52 | mm |
| Tube spacing | 25.4 | mm |
| Fin spacing | 2.12 | mm |
| Fin thickness | 0.127 | mm |
| Number of tube rows | 2 | – |
| Number of tubes in each row | 10 | – |
| Fin type | shutters | – |

For solution heat exchange, the Shell-and-Tube exchangers are adopted in the proposed system. The inner and outer diameters of the tubes are 16 mm and 19 mm, respectively. Also, the coil length may vary for changing the heat exchange area to meet different working conditions. The detailed geometry for solution heat exchangers are given in [Table A2](#).

Table A2
Main geometry of solution heat exchangers

| Item | Values | Unit |
|------------------------------|--------|------|
| <i>Shell side parameters</i> | | |
| Tube outside diameter | 19 | mm |
| Tube inside diameter | 16 | mm |
| Tube pitch, square lay out | 25 | mm |

(continued on next page)

Table A2 (continued)

| Item | Values | Unit |
|--------------------------|----------|------|
| Tube wall thickness | 1.5 | mm |
| Arranging type for tubes | Triangle | — |
| <i>Baffle parameters</i> | | |
| Width of plate | 62.5 | mm |
| Plate pitch | 62.5 | mm |
| Number of passes | 2 | — |

The finned coil structure is used in the absorber, and the packing density of the thermally conductive Celdek plastic pads are 396 m²/m³. The cooling coil is made of aluminum tubes, arranged in 8 rows and 6 passes. An internal-heated vacuum regenerator is adopted in this paper, in which diluted solution is regenerated through the boiling process. Specification of absorber and regenerator in presented study are given in Table A3.

Table A3

Specification of absorber and regenerator in presented study

| | Flow pattern | Size | Type | Desiccant | Pressure (Pa) |
|-------------|--------------|-----------------------|-------------------------------|-----------|------------------------|
| Absorber | Cross flow | 1.1 m × 0.7 m × 0.8 m | Celdek and fin-coil structure | LiBr | 1.01 × 10 ⁵ |
| Regenerator | Falling film | 1.2 m × 0.8 m × 0.6 m | Horizontal tubes and vacuum | LiBr | 4780 |

References

- [1] B. Dai, P. Zhao, S. Liu, et al., Assessment of heat pump with carbon dioxide/low-global warming potential working fluid mixture for drying process: energy and emissions saving potential[J], *Energy Convers. Manag.* 222 (2020), 113225.
- [2] C. Wang, J. Song, W. Zheng, et al., Analysis of economy, energy efficiency, environment: A case study of the CHP system with both civil and industrial heat users [J], *Case Stud. Therm. Eng.* 30 (2022), 101768.
- [3] C. Gu, Y. Zhang, C. Tang, et al., Research on synchronous optimization effect of working fluid components and node parameters of organic Rankine cycle (ORC) [J], *Case Stud. Therm. Eng.* 30 (2022), 101742.
- [4] L.J. Goh, M.Y. Othman, S. Mat, et al., Review of heat pump systems for drying application[J], *Renew. Sustain. Energy Rev.* 15 (9) (2011) 4788–4796.
- [5] M. Ahmad, K.R. Gluesenkamp, S. Bigham, Energy-efficient sorption-based gas clothes dryer systems[J], *Energy Convers. Manag.* 230 (2021), 113763.
- [6] R. Daghigh, A. Shafieian, An experimental study of a heat pipe evacuated tube solar dryer with heat recovery system[J], *Renew. Energy* 96 (2016) 872–880.
- [7] A.A. El-Sabaii, S.M. Shalaby, Experimental investigation of an indirect-mode forced convection solar dryer for drying thymus and mint[J], *Energy Convers. Manag.* 74 (2013) 109–116.
- [8] B. Dai, P. Zhao, S. Liu, et al., Assessment of heat pump with carbon dioxide/low-global warming potential working fluid mixture for drying process: energy and emissions saving potential[J], *Energy Convers. Manag.* 222 (2020), 113225.
- [9] M. Aktaş, S. evik, M.B. özdemir, et al., Performance analysis and modeling of a closed-loop heat pump dryer for bay leaves using artificial neural network[J], *Appl. Therm. Eng.* 87 (2015) 714–723.
- [10] M. Kuan, Y. Shakir, M. Mohanraj, et al., Numerical simulation of a heat pump assisted solar dryer for continental climates[J], *Renew. Energy* 143 (2019) 214–225.
- [11] A. Singh, J. Sarkar, R. Rekha Sahoo, Experimentation on solar-assisted heat pump dryer: thermodynamic, economic and exergoeconomic assessments[J], *Sol. Energy* 208 (2020) 150–159.
- [12] A. Singh, J. Sarkar, R.R. Sahoo, Experimental performance analysis of novel indirect-expansion solar-infrared assisted heat pump dryer for agricultural products [J], *Sol. Energy* 206 (2020) 907–917.
- [13] M. Aktaş, L. Taseri, S. evik, et al., Heat pump drying of grape pomace: performance and product quality analysis[J], *Dry. Technol.* 37 (14) (2019) 1766–1779.
- [14] Z. Li, W. Wu, J. Wang, et al., Effect of compressor speeds on performance of a closed loop heat pump drying system[J], *Appl. Therm. Eng.* 195 (2021), 117220.
- [15] I. T'Jollyn, S. Lecompte, B. Vanslambrouck, et al., Energetic and financial assessment of the implementation of an absorption heat pump in an industrial drying system[J], *Dry. Technol.* 37 (15) (2019) 1939–1953.
- [16] C. Liu, Y. Jiang, W. Han, et al., A high-temperature hybrid absorption-compression heat pump for waste heat recovery[J], *Energy Convers. Manag.* 172 (2018) 391–401.
- [17] Q. Duan, D. Wang, X. Li, et al., Thermal characteristics of a novel enclosed cascade-like heat pump dryer used in a tunnel type drying system[J], *Appl. Therm. Eng.* 155 (2019) 206–216.
- [18] M. Aktaş, A. Khanlari, A. Amini, et al., Performance analysis of heat pump and infrared–heat pump drying of grated carrot using energy-exergy methodology[J], *Energy Convers. Manag.* 132 (2017) 327–338.
- [19] S. evik, M. Aktaş, H. Doğan, et al., Mushroom drying with solar assisted heat pump system[J], *Energy Convers. Manag.* 72 (2013) 171–178.
- [20] Q. Shi, Y. Zheng, Y. Zhao, Mathematical modeling on thin-layer heat pump drying of yacon (*Smallanthus sonchifolius*) slices[J], *Energy Convers. Manag.* 71 (2013) 208–216.
- [21] K. Chapchaimoh, N. Poomsa-Ad, L. Wiset, et al., Thermal characteristics of heat pump dryer for ginger drying[J], *Appl. Therm. Eng.* 95 (2016) 491–498.
- [22] W. Tegrotenhuis, A. Butterfield, D. Caldwell, et al., Modeling and design of a high efficiency hybrid heat pump clothes dryer[J], *Appl. Therm. Eng.* 124 (2017) 170–177.
- [23] J. Cranston, A. Asklany, G. Santori, Efficient drying in washer dryers by combining sorption and heat pumping[J], *Energy* 183 (2019) 683–692.
- [24] M. Dorouzi, H. Mortezapour, H. Akhavan, et al., Tomato slices drying in a liquid desiccant-assisted solar dryer coupled with a photovoltaic-thermal regeneration system[J], *Sol. Energy* 162 (2018) 364–371.
- [25] H. Atalay, Comparative assessment of solar and heat pump dryers with regards to exergy and exergoeconomic performance[J], *Energy* 189 (2019), 116180.
- [26] Z.Y. Xu, J.T. Gao, H.C. Mao, et al., Double-section absorption heat pump for the deep recovery of low-grade waste heat[J], *Energy Convers. Manag.* 220 (2020), 113072.
- [27] Z. Wang, X. Zhang, J. Han, et al., Waste heat and water recovery from natural gas boilers: parametric analysis and optimization of a flue-gas-driven open absorption system[J], *Energy Convers. Manag.* 154 (2017) 526–537.
- [28] H. Zhang, Y. Dong, Y. Lai, et al., Waste heat recovery from coal-fired boiler flue gas: performance optimization of a new open absorption heat pump[J], *Appl. Therm. Eng.* 183 (2021), 116111.

- [29] W. Su, X. Zhang, Performance analysis of a novel frost-free air-source heat pump with integrated membrane-based liquid desiccant dehumidification and humidification[J], *Energy Build.* 145 (2017) 293–303.
- [30] C. Zhang, Y. Zhao, X. Shi, et al., Characterization of a new total heat recovery system using CaCl₂ as working fluid: thermal modeling and physical analysis[J], *Energy. Built Environ.* 3 (2) (2020) 158–170, <https://doi.org/10.1016/j.enbenv.2020.12.003>.
- [31] Y. Wang, S. Yang, Proposal and thermodynamic analysis of a combined open-cycle absorption heat pump and thermal desalination system driven by high-humidity exhaust gas[J], *Desalination* 448 (2018) 93–102.
- [32] X. Wang, J. Zhuo, J. Liu, et al., Synergetic process of condensing heat exchanger and absorption heat pump for waste heat and water recovery from flue gas[J], *Appl. Energy* 261 (2020), 114401.
- [33] B. Yang, W. Yuan, L. Fu, et al., Techno-economic study of full-open absorption heat pump applied to flue gas total heat recovery, *J. Energy* 190 (2020), 116429.
- [34] E. Oktariani, K. Tahara, K. Nakashima, et al., Experimental investigation on the Adsorption process for steam generation using a zeolite–water system[J], *J. Chem. Eng. Jpn.* 45 (5) (2012) 355–362.
- [35] B. Xue, K. Tahara, K. Nakashima, et al., Numerical simulation for steam generation process in a novel zeolite–water adsorption heat pump[J], *J. Chem. Eng. Jpn.* 45 (6) (2012) 408–416.
- [36] W. Su, Z. Lu, X. She, et al., Liquid desiccant regeneration for advanced air conditioning: A comprehensive review on desiccant materials, regenerators, systems and improvement technologies[J], *Appl. Energy* 308 (2022), 118394.
- [37] W. He, X. Hong, X. Zhao, et al., Operational performance of a novel heat pump assisted solar façade loop-heat-pipe water heating system[J], *Appl. Energy* 146 (2015) 371–382.
- [38] J. Liu, X. Liu, T. Zhang, Performance comparison of three typical types of internally-cooled liquid desiccant dehumidifiers[J], *Build. Environ.* 103 (2016) 134–145.
- [39] X.H. Liu, X.M. Chang, J.J. Xia, et al., Performance analysis on the internally cooled dehumidifier using liquid desiccant[J], *Build. Environ.* 44 (2) (2009) 299–308.
- [40] W. Su, H. Li, B. Sun, et al., Performance investigation on a frost-free air source heat pump system employing liquid desiccant dehumidification and compressor-assisted regeneration based on exergy and exergoeconomic analysis[J], *Energy Convers. Manag.* 183 (2019) 167–181.
- [41] M.A. Jamil, S.M. Zubair, Effect of feed flow arrangement and number of evaporators on the performance of multi-effect mechanical vapor compression desalination systems[J], *Desalination* 429 (2018) 76–87.
- [42] O. Brunin, M. Feidt, B. Hivet, Comparison of the working domains of some compression heat pumps and a compression-absorption heat pump[J], *Int. J. Refrig.* 20 (5) (1997) 308–318.
- [43] L. Zhang, X. Liu, Y. Jiang, Exergy analysis of parameter unmatched characteristic in coupled heat and mass transfer between humid air and water[J], *Int. J. Heat Mass Tran.* 84 (2015) 327–338.
- [44] L. Zhang, X. Liu, J. Jiang, et al., Exergy calculation and analysis of a dehumidification system using liquid desiccant[J], *Energy Build.* 69 (2014) 318–328.
- [45] C. Wu, S. Wang, X. Feng, et al., Energy, exergy and exergoeconomic analyses of a combined supercritical CO₂ recompression Brayton/absorption refrigeration cycle[J], *Energy Convers. Manag.* 148 (2017) 360–377.
- [46] M.A. Jamil, S.M. Zubair, Design and analysis of a forward feed multi-effect mechanical vapor compression desalination system: An exergo-economic approach [J], *Energy* 140 (2017) 1107–1120.
- [47] W. Su, W. Li, X. Zhang, Simulation analysis of a novel no-frost air-source heat pump with integrated liquid desiccant dehumidification and compression-assisted regeneration[J], *Energy Convers. Manag.* 148 (2017) 1157–1169.
- [48] Q. Cui, E. Gao, Z. Zhang, et al., Preliminary study on the feasibility assessment of CO₂ booster refrigeration systems for supermarket application in China: An energetic, economic, and environmental analysis[J], *Energy Convers. Manag.* 225 (2020), 113422.
- [49] K.R. Patil, A.D. Tripathi, G. Pathak, et al., Thermodynamic properties of aqueous electrolyte solutions. 1. Vapor pressure of aqueous solutions of lithium chloride, lithium bromide, and lithium iodide[J], *J. Chem. Eng. Data* 35 (2) (1990) 166–168.
- [50] M.M. Rafique, P. Gandhisadasan, H.M.S. Bahadharah, Liquid desiccant materials and dehumidifiers – A review[J], *Renew. Sustain. Energy Rev.* 56 (2016) 179–195.
- [51] <https://www.opteon.com/en/products/refrigerants/xp30>.
- [52] NIST Reference Fluid Thermodynamic and Transport Properties Database(REFPROP): Version 9.1.
- [53] J. Liu, T. Zhang, X. Liu, et al., Experimental analysis of an internally-cooled/heated liquid desiccant dehumidifier/regenerator made of thermally conductive plastic[J], *Energy Build.* 99 (2015) 75–86.
- [54] X. She, Y. Yin, Y. Luo, et al., Experimental study of a novel subcooling method based on liquid desiccant dehumidification for vapor-compression refrigeration systems[J], *Appl. Therm. Eng.* 130 (2018) 1460–1471.
- [55] O.A. Khatchatourian, H.A. Vielmo, L.A. Bortolaia, Modelling and simulation of cross flow grain dryers[J], *Biosyst. Eng.* 116 (4) (2013) 335–345.
- [56] S. Mehran, M. Nikian, M. Ghazi, et al., Experimental investigation and energy analysis of a solar-assisted fluidized-bed dryer including solar water heater and solar-powered infrared lamp for paddy grains drying[J], *Sol. Energy* 190 (2019) 167–184.
- [57] H.T. Jokiniemi, J.M. Ahokas, Drying process optimisation in a mixed-flow batch grain dryer[J], *Biosyst. Eng.* 121 (2014) 209–220.
- [58] W. Su, W. Li, B. Sun, et al., Experimental study and correlations for heat and mass transfer coefficients in the dehumidifier of a frost-free heat pump system[J], *Int. J. Heat Mass Tran.* 131 (2019) 450–462.